Published by Institute of Physics Publishing for SISSA

Received: *September 20, 2007*
Accepted: *November 14, 2007*
Published: *December 3, 2007*

Probing non-standard neutrino interactions with neutrino factories

N. Cipriano Ribeiro,[a] **H. Minakata,**[b] **H. Nunokawa,**[a] **S. Uchinami**[b] **and R. Zukanovich Funchal**[c]

[a] *Departamento de Física, Pontifícia Universidade Católica do Rio de Janeiro, Rua Marquês de São Vicente 225 - Gávea, C. P. 38071, 22452-970, Rio de Janeiro, Brazil*
[b] *Department of Physics, Tokyo Metropolitan University, Hachioji, Tokyo 192-0397, Japan*
[c] *Instituto de Física, Universidade de São Paulo, Rua do Matão, Travessa R, 187, Cidade Universitária, C. P. 66.318, 05315-970 São Paulo, Brazil*
E-mail: ncipriano@fis.puc-rio.br, minakata@phys.metro-u.ac.jp, nunokawa@fis.puc-rio.br, uchinami@phys.metro-u.ac.jp, zukanov@if.usp.br

Abstract: We discuss the sensitivity reach of a neutrino factory measurement to non-standard neutrino interactions (NSI), which may exist as a low-energy manifestation of physics beyond the Standard Model. We use the muon appearance modes $\nu_e \to \nu_\mu/\bar{\nu}_e \to \bar{\nu}_\mu$ and consider two detectors, one at $L = 3000$ km and the other at $L = 7000$ km; The latter is nearly at the magic baseline which is known to have a great sensitivity to matter density determination. Assuming the effects of NSI at the production and the detection are negligible, we discuss the sensitivities to NSI and the simultaneous determination of θ_{13} and δ by examining the effects in the neutrino propagation of various systems in which two NSI parameters $\varepsilon_{\alpha\beta}$ are switched on. The sensitivities to off-diagonal ε's are found to be excellent up to small values of θ_{13}. At $\sin^2 2\theta_{13} = 10^{-4}$, for example, $|\varepsilon_{e\tau}| \simeq$ a few $\times 10^{-3}$ at 3σ CL for 2 degrees of freedom, whereas the ones for the diagonal ε's are also acceptable, $|\varepsilon_{ee}|(|\varepsilon_{\tau\tau}|) \simeq 0.1(0.2)$ at the same CL. We demonstrate that the two-detector setting is powerful enough to resolve the θ_{13}-NSI confusion problem, a notorious one which is thought to be an obstacle in determining θ_{13} and δ. We believe that the results obtained in this paper open the door to the possibility of using neutrino factory as a discovery machine for NSI while keeping its primary function of performing precision measurements of the lepton mixing parameters.

Keywords: Neutrino Physics, Beyond Standard Model.

JHEP12(2007)002

Contents

1. Introduction

In the last 10 years various neutrino experiments made it clear that neutrinos have masses and lepton flavors mix [1, 2]. Though the measurement of the values of θ_{13} and the CP phase δ as well as determining the neutrino mass hierarchy still elude us, there exist an array of experimental plans and ideas to make the goal. If successful they will bring us a more or less complete picture of how neutrinos organize their mass spectrum and how lepton flavors mix. When it happens, then, we will really be entering into the era of precision measurement of lepton mixing parameters. An intriguing question is whether this will serve just for precision measurements of more or less known quantities, or could help us to discover new physics beyond the Standard Model which is amended to incorporate neutrino masses and mixing.

It has been suggested since long time ago that neutrinos may have non-standard interactions (NSI) in addition to those dictated by the Standard Model of electroweak interactions [3 – 6]. If there exists an energy scale for new physics at the TeV range, it is conceivable that it produces higher dimension operators which affect the way how neutrinos interact with matter, the point raised in [7]. It was argued that such NSI possessed by neutrinos need not be subject to the stringent constraints that the charged leptons have to obey [8]. The existing constraints on NSI for neutrinos are worked out in [9, 10]. If we follow naive dimensional counting with four Fermi operators the order of magnitude of NSI is expected to be $(m_Z/M_{\rm NSI})^2 \sim 10^{-2}$ ($\sim 10^{-4}$) for the energy scale of new physics $M_{\rm NSI}$ of ~ 1 (10) TeV [11]. If we want to probe into such a tiny effect of NSI in the neutrino sector, extremely high sensitivities are required for experiments to detect deviations from the standard three flavor oscillations. A large number of papers in the literature is devoted to discuss NSI in various context including long-baseline accelerator experiments, the atmospheric and the solar neutrino observations, and supernova neutrinos [11 – 26].

It is the purpose of this paper to discuss the discovery potential of NSI in a neutrino factory. As is well known, a neutrino factory [27] is an ultimate apparatus for precision measurements of the lepton mixing parameters. Because of the capability of clean detection of muons including the charge identification, its sensitivity to θ_{13} is expected to go down to an extremely small value, somewhere in the range $\sin^2 2\theta_{13} = 10^{-5} - 10^{-4}$ [28 – 30]. Then, it is natural to think about neutrino factory as a discovery machine for NSI.

One of the key issues in the discussion of the discovery reach of NSI is that we have to guarantee, at the same time, the ability of accurately measure the lepton mixing parameters, especially θ_{13} and δ, is left intact. However, it is a difficult goal to achieve in particular when we go down to very small values of θ_{13} and NSI contributions. In fact, it is known that the presence of NSI can confuse the measurement of θ_{13} by mimicking its effect [13, 14]. Unless this problem is somehow solved, it is difficult to think about a neutrino factory as a sensitive hunting tool for NSI and at the same time as a viable apparatus for precision measurements of the lepton mixing parameters.

We do overcome the confusion problem by our set-up. We consider a two detector setting with baselines at $L = 3000$ km and at $L = 7000$ km [13], which will sometimes be referred as the intermediate and the far detectors, respectively. Comparing the yields

taken by the two detectors is the key to resolve the confusion. These features will be demonstrated in sections 5 and 6. We must note, however, that it is only by keeping the solar Δm^2 terms that one can gain access to the CP phase δ which is crucial to resolve the muddle between θ_{13} and NSI. Therefore, we keep the solar Δm^2 terms throughout our analytical and numerical treatment.

If the two detector setting is a special requirement for hunting NSI it would not be easy to implement it into the project. Fortunately, it is *not* the case. It has been suggested [31, 32] that combining measurements by detectors at two baselines, one at 3000-4000 km and the other at ∼7000 km, is powerful enough to resolve the parameter degeneracy [31, 33, 34] associated with the measurement of the lepton mixing parameters, a notorious obstacle to its precision determination. The power of the two detector setting has been confirmed also by more recent analysis [35].

In section 2, we present the general framework for probing NSI through neutrino propagation in matter by switching on two NSI contributions simultaneously and discuss some important points about NSI effects in the $P(\nu_e \to \nu_\mu)/P(\bar{\nu}_e \to \bar{\nu}_\mu)$ oscillation probabilities, the channels explored in this paper. In section 3, we elucidate the powerfulness of the strategy to look for NSI in a neutrino factory by combining the measurements of two identical detectors at different baselines. The assumptions we make about the neutrino factory parameters and the two detector setup as well as the analysis we perform are described in section 4. In section 5, we discuss the maximal sensitivity to the various combinations of NSI parameters and their effects on the precision measurements of the oscillation parameters δ and θ_{13}. In section 6 we discuss the accuracy of the determination of the NSI parameters as well as their impact on the measurement of δ and θ_{13} in the case they are sufficiently large to be measured by the neutrino factory experiment. The discovery reach to NSI, δ and θ_{13} is presented in section 7. Section 8 is devoted to our final concluding remarks. In appendix A, we give details on the derivation of the appearance probability $P(\nu_e \to \nu_\mu)$ in the presence of two NSI parameters.

2. Non-standard interactions of neutrinos

2.1 General features

We consider NSI involving neutrinos of the type

$$\mathcal{L}_{\rm eff}^{\rm NSI} = -2\sqrt{2}\,\varepsilon_{\alpha\beta}^{fP} G_F (\overline{\nu}_\alpha \gamma_\mu P_L \nu_\beta)\,(\overline{f}\gamma^\mu P f), \tag{2.1}$$

where G_F is the Fermi constant, and f stands for the index running over fermion species in the earth, $f = e, u, d$, in which we follow [9] for notation. P stands for a projection operator and is either $P_L \equiv \frac{1}{2}(1-\gamma_5)$ or $P_R \equiv \frac{1}{2}(1+\gamma_5)$. We summarize here the bounds on $\varepsilon_{\alpha\beta}^{fP}$ which are obtained in [9, 10] for the readers convenience:

$$\begin{bmatrix} -0.9 < \varepsilon_{ee} < 0.75 & |\varepsilon_{e\mu}| \lesssim 3.8\times 10^{-4} & |\varepsilon_{e\tau}| \lesssim 0.25 \\ & -0.05 < \varepsilon_{\mu\mu} < 0.08 & |\varepsilon_{\mu\tau}| \lesssim 0.25 \\ & & |\varepsilon_{\tau\tau}| \lesssim 0.4 \end{bmatrix}, \tag{2.2}$$

bounds from Davidson *et al.* (LEP) are at 90% (95%) CL.

In this paper, we consider the effect of NSI in neutrino propagation in matter. It is known that NSI can affect production and detection processes of neutrinos so that a complete treatment must involve also the latter two effects. However, we should note that the muon storage ring which we assume as a source of neutrinos is special as it is one of the cleanest. Muon decay has been studied with great precision and room for NSI is smallest among the sources [36]. Because construction of the muon storage ring will require an intense muon source, we assume that the already tight constraints on NSI by muon decay would become much more stringent at that time. Therefore, we believe that to neglect NSI in the production of neutrinos in fact gives a fair approximation, unless we go down to extremely small values of $\varepsilon_{\alpha\beta}$.

With regard to NSI at the detection this may be more debatable. However, we call the readers' attention to the fact that upon construction of the neutrino factory the near detector sitting in front of the storage ring will give a severe bound on NSI [9]. We also remark that even before that era several low energy neutrino experiments may be able to place equally severe constraints on NSI [37 – 39]. The bounds from them are placed on the product of NSI at the source and the detection. But if the constraint on NSI by muon decays is strongly constrained, this will translate into a stringent bound on NSI at the detection. Furthermore, since we compare two identical detectors, at the intermediate ($L = 3000$ km) and the far ($L = 7000$ km) location, the NSI effect at detectors tend to cancel. Therefore, our approximation of ignoring NSI at the detection points may give a reasonable first approximation.

To discuss the effects of NSI during neutrino propagation in matter we will use the effective coefficients $\varepsilon_{\alpha\beta}$ as it is traditional in this field. They are defined as $\varepsilon_{\alpha\beta} \equiv \sum_{f,P} \frac{n_f}{n_e} \varepsilon^{\rm fP}_{\alpha\beta}$. where n_f is the number density of the fermion species f in matter. Normalizing by the electron number density n_e leads to a simple structure of the effective Hamiltonian which governs the neutrino propagation in matter. Approximately, the relation $\varepsilon_{\alpha\beta} \simeq \sum_P \left(\varepsilon^{\rm eP}_{\alpha\beta} + 3\,\varepsilon^{\rm uP}_{\alpha\beta} + 3\,\varepsilon^{\rm dP}_{\alpha\beta} \right)$ holds because of a factor of $\simeq$3 larger number of u and d quarks than electrons in iso-singlet matter.

The time evolution of neutrinos in flavor basis with non-standard neutrino matter interactions can be generically written as

$$i\frac{d}{dt}\begin{pmatrix}\nu_e\\ \nu_\mu\\ \nu_\tau\end{pmatrix} = \frac{1}{2E}\left[U\begin{pmatrix}0 & 0 & 0\\ 0 & \Delta m^2_{21} & 0\\ 0 & 0 & \Delta m^2_{31}\end{pmatrix}U^\dagger + a\begin{pmatrix}1+\varepsilon_{\rm ee} & \varepsilon_{e\mu} & \varepsilon_{e\tau}\\ \varepsilon^*_{e\mu} & \varepsilon_{\mu\mu} & \varepsilon_{\mu\tau}\\ \varepsilon^*_{e\tau} & \varepsilon^*_{\mu\tau} & \varepsilon_{\tau\tau}\end{pmatrix}\right]\begin{pmatrix}\nu_e\\ \nu_\mu\\ \nu_\tau\end{pmatrix} \quad (2.3)$$

where U is the Maki-Nakagawa-Sakata (MNS) [1] matrix, and $a \equiv 2\sqrt{2}G_F n_e E$ [3] where E is the neutrino energy and n_e denotes the electron number density along the neutrino trajectory in the earth. $\Delta m^2_{ij} \equiv m^2_i - m^2_j$ with neutrino mass m_i ($i = 1 - 3$). Eq. (2.3) defines the framework for discussing neutrino propagation in matter with NSI.

2.2 Physics of neutrino propagation in matter with NSI; two ε system

In this paper, we will be dealing with the cases where the following pairs of ε parameters are present at the same time: $\varepsilon_{e\tau} - \varepsilon_{ee}$, $\varepsilon_{e\tau} - \varepsilon_{\tau\tau}$, $\varepsilon_{\tau\tau} - \varepsilon_{ee}$, $\varepsilon_{e\mu} - \varepsilon_{\rm ee}$, $\varepsilon_{e\mu} - \varepsilon_{\tau\tau}$, and

$\varepsilon_{e\tau} - \varepsilon_{e\mu}$. The systems with many ε's are complicated enough and a step by step approach is needed to grasp the whole picture. In appendix A, we will derive the exact expressions and the approximate formulas for the appearance oscillation probabilities $P(\nu_e \to \nu_\mu)$ in the two systems $\varepsilon_{e\tau} - \varepsilon_{ee}$ and $\varepsilon_{e\mu} - \varepsilon_{ee}$. To obtain tractable formulas we use perturbation expansion in terms of small parameters, $s_{13} \simeq \delta_{21} \simeq \varepsilon_{e\tau}$ (or $\varepsilon_{e\mu}$) which we assume to have comparable sizes $\sim 10^{-2}$, where δ_{21} is defined in appendix A. For simplicity, we collectively denote their order of magnitude as ϵ under the hope that no confusion arises with the NSI elements $\varepsilon_{\alpha\beta}$. See [11, 14, 15, 26, 40] for different treatment of the perturbation series. We will observe that in leading order the appearance oscillation probabilities $P(\nu_e \to \nu_\mu)$ are of order ϵ^2. Of course, it reduces to the Cervera *et al.* formula [28] if $\varepsilon_{\alpha\beta}$ are switched off.

We mention some notable features of the leading order formulas of $P(\nu_e \to \nu_\mu)$ in (A.25) and (A.27), and make comments for better understanding of our results. To discuss simultaneously the $\varepsilon_{e\tau} - \varepsilon_{ee}$ and $\varepsilon_{e\mu} - \varepsilon_{ee}$ systems, we use the notation $\varepsilon_{\alpha\beta}$ for (α, β) is either $(e\mu)$ or $(e\tau)$. Since an off-diagonal element of ε can have CP violating phase we have a new source for CP violation in addition to δ in the MNS matrix, as emphasized in [11] in a somewhat different framework. In this context we notice that $\varepsilon_{\alpha\beta}$ comes in via three different ways:

(a) $\varepsilon_{\alpha\beta}$ comes into the formula with its phase, $\phi_{\alpha\beta}$, in the form $\delta + \phi_{\alpha\beta}$ together with the leptonic Kobayashi-Maskawa (KM) phase δ in the MNS matrix. [15, 25].

(b) $\varepsilon_{\alpha\beta}$ comes in by itself, i.e., in the form of $\mathrm{Re}(\varepsilon_{\alpha\beta})$ or $\mathrm{Im}(\varepsilon_{\alpha\beta})$.

(c) $\varepsilon_{\alpha\beta}$ comes in by the absolute magnitude squared, $|\varepsilon_{\alpha\beta}|^2$ without phase.

Terms of the type (a) and (c) survive even when the solar Δm^2_{21} is turned off, whereas terms of the type (b) arise only when they are accompanied by the solar Δm^2_{21}.

We suggest an intuitive understanding of the fact that two phases come together when Δm^2_{21} is switched off. The system without Δm^2_{21} contains effectively only two generations of neutrinos and on physics ground the CP violating phase should be unique. Therefore, the phase of $\varepsilon_{\alpha\beta}$ and the KM phase δ must come together. From this reasoning, we suspect that this feature holds even in the exact formula. Of course, the two phases start to play their individual roles when the solar Δm^2_{21} is turned on, as in the form of (b) above and the second line of the Cervera *et al.* formula (A.26), as seen in (A.25) and (A.27).

Due to the special way through which the phase of $\varepsilon_{\alpha\beta}$ enters into the oscillation probability in the absence of the solar Δm^2_{21}, we expect that confusions occur in the experimental settings for which ignoring the solar Δm^2_{21} gives a fair approximation. We expect two types of confusion to occur:

- Two phase confusion: Since they appear in the special combination $\phi_{\alpha\beta} + \delta$, it is obvious that two phase confusion occurs; the data allows determination of only the sum. The confusion cannot be resolved even if the anti-neutrino channel is combined. It can be resolved for relatively large $|\varepsilon_{\alpha\beta}|$ because the terms with Δm^2_{21} start to play more important role. These features are in fact observed for $\varepsilon_{e\mu}$ in [25]. We note that the symmetry under simultaneous shift of $\phi_{\alpha\beta}$ and δ by the same amount but with

opposite signs is a symmetry of the whole system at the magic baseline. We will see that this confusion shows up in our analysis. (See sections 5 and 6.)

- Phase-magnitude confusion: We expect that another type of confusion exists. The term which contains the phases in (A.25) and (A.27) take the form

$$A|\varepsilon_{\alpha\beta}|\cos(\phi_{\alpha\beta}+\delta)+B|\varepsilon_{\alpha\beta}|\sin(\phi_{\alpha\beta}+\delta)=|\varepsilon_{\alpha\beta}|\sqrt{A^2+B^2}\cos(\phi_{\alpha\beta}+\delta-\xi)\,, \quad (2.4)$$

where $\tan\xi = B/A$. Therefore, varying the magnitude of the NSI element can be compensated by adjusting the phase of $\varepsilon_{\alpha\beta}$. Unlike the two phase confusion, this confusion can in principle be resolved if (1) $|\varepsilon_{\alpha\beta}|^2$ terms are important enough to resolve the confusion, and/or (2) the anti-neutrino channel is combined, because the coefficients A and B are different between neutrino and anti-neutrino oscillation probabilities.

3. Probing NSI by detectors at two baselines; their characteristics and synergy

In this section, we indicate by qualitative level arguments that the $\nu_\mu/\bar{\nu}_\mu$ appearance measurement in neutrino factory at the magic baseline,

$$L=\frac{\sqrt{2}\pi}{G_F n_e}=7200\left(\frac{\rho}{4.5\ \mathrm{g/cm^3}}\right)^{-1}\mathrm{km}\,, \quad (3.1)$$

and the synergy obtained when combined with measurement at $L \simeq 3000$ km provide a powerful method for probing non-standard neutrino-matter interactions. Powerfulness of the measurement at the magic baseline may be natural to expect for $\varepsilon_{\mathrm{ee}}$ because it is effectively equivalent to measuring the electron number density in earth matter for which the accuracy of determination is known to be excellent [41, 42]. We show in this paper that this statement is even more true for flavor off-diagonal NSI. We rely on $\nu_e \to \nu_\mu/\bar{\nu}_e \to \bar{\nu}_\mu$ appearance channels, the so called golden channels [28], because of the matured muon detection technology.

3.1 Detector at the magic baseline as a sensitive probe to NSI

To illuminate that measurement at the magic baseline is a powerful indicator for NSI, in particular for off-diagonal $\varepsilon_{\alpha\beta}$, we present in figure 1 the ellipses formed when δ is varied in the bi-probability space spanned by $P(\nu_e \to \nu_\mu)$ and $P(\bar{\nu}_e \to \bar{\nu}_\mu)$ [33] for various non-zero NSI parameters. The calculation was performed numerically assuming the constant matter density $\rho = 4.5$ g/cm^3. In each panel only the indicated particular $\varepsilon_{\alpha\beta}$ is turned on. Also shown in figure 1 as an orange strip is the region covered by the ellipses when θ_{13} is varied for the cases without NSI. It approximately forms a narrow straight strip (or "pencil") because of vanishingly small effect of δ at the magic baseline [43]. The remarkable feature of figure 1 is that the effect of NSI in the neutrino and the anti-neutrino probabilities is large for electron-type off-diagonal terms, $\varepsilon_{e\tau}$ and $\varepsilon_{e\mu}$, even though their size is extremely small, $\varepsilon_{e\mu} = \varepsilon_{e\tau} = 10^{-3}$. Notice that the sizes of the other ε's which give rise to effect of

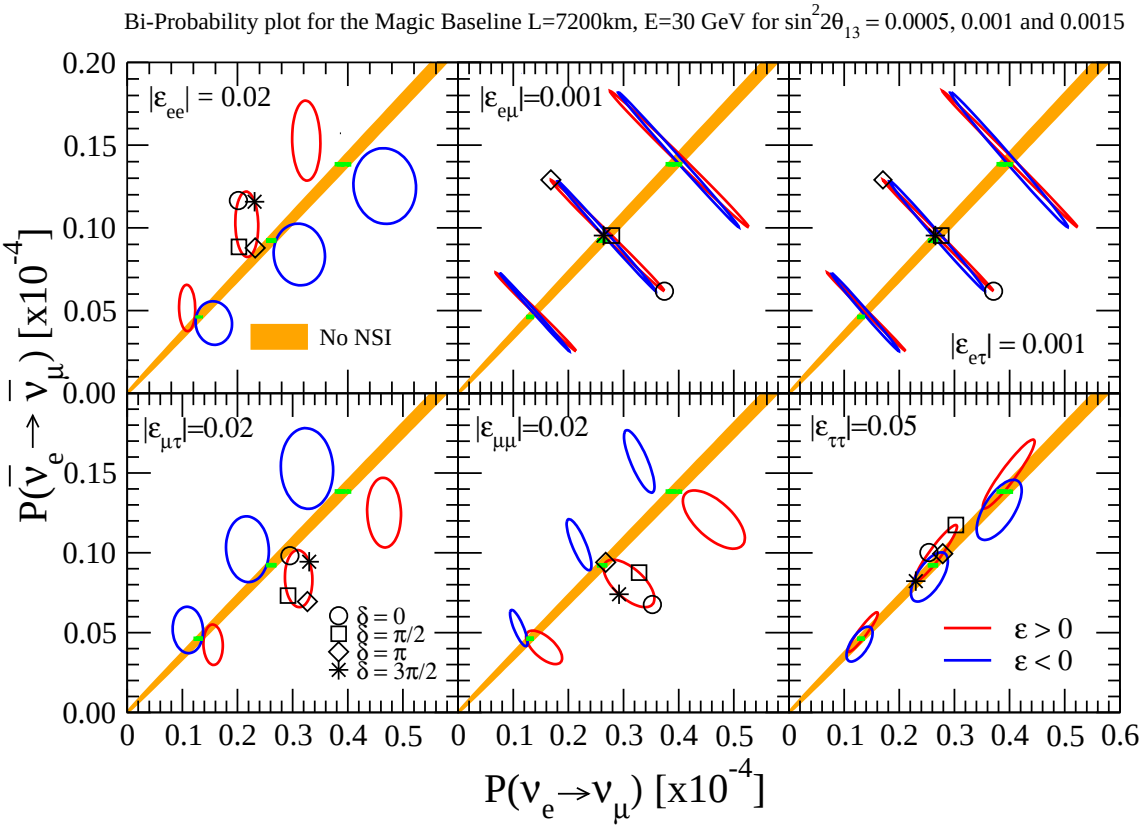

Figure 1: Bi-probability plots in $P(\nu_e \to \nu_\mu) - P(\bar{\nu}_e \to \bar{\nu}_\mu)$ space at the magic baseline, $L = 7200$ km, for $E = 30\,\text{GeV}$, computed numerically using the constant matter density $\rho = 4.5\ \text{g/cm}^3$ with the electron number density per nucleon equals to 0.5. The both axes is labeled in units of 10^{-4}. In each panel only the indicated particular $\varepsilon_{\alpha\beta}$ is turned on. The upper (lower) panels, from left to right, correspond to the case of non-vanishing ε_{ee}, $\varepsilon_{e\mu}$, and $\varepsilon_{e\tau}$ ($\varepsilon_{\mu\tau}$, $\varepsilon_{\mu\mu}$, $\varepsilon_{\tau\tau}$), respectively. The red and the blue ellipses are for positive and negative signs of ε, respectively, for the cases with (from left to right) $\sin^2 2\theta_{13} = 0.0005$, 0.001, and 0.0015, as indicated in the heading. The values of the non-vanishing ε are written in each panel. The orange colored region indicates the region spanned by ellipses without NSI when θ_{13} is varied. The green dots are unresolved ellipses corresponding to the same values of $\sin^2 2\theta_{13}$ but without NSI. The values of the standard lepton mixing parameters are given in the caption of figure 3. Only for the case of $\varepsilon > 0$ and $\sin^2 2\theta_{13} = 0.001$ we show the position corresponding to the four different values of $\delta = 0, \pi/2, \pi$ and $3\pi/2$ by the open circle, square, diamond and asterisk, respectively.

similar magnitude as those of $\varepsilon_{e\mu}$ and $\varepsilon_{e\tau}$ are larger by a factor of 20 ($\varepsilon_{\mu\tau}$ and $\varepsilon_{\mu\mu}$) and of > 50 ($\varepsilon_{\tau\tau}$). This is the key point of our setting which allows the extremely high sensitivity to $\varepsilon_{e\tau}$ and $\varepsilon_{e\mu}$.

There are some curious features in figure 1; The behavior of the ellipses with $\varepsilon_{e\tau}$ and $\varepsilon_{e\mu}$ are distinct from the other cases having ellipses shrunk forming almost lines. At the same time it is also notable that they look almost identical to each other. Let us understand these characteristic features of figure 1.

In appendix A we derive the leading order formula for $P(\nu_e \to \nu_\mu)$ with $\varepsilon_{e\tau}$ or $\varepsilon_{e\mu}$ as

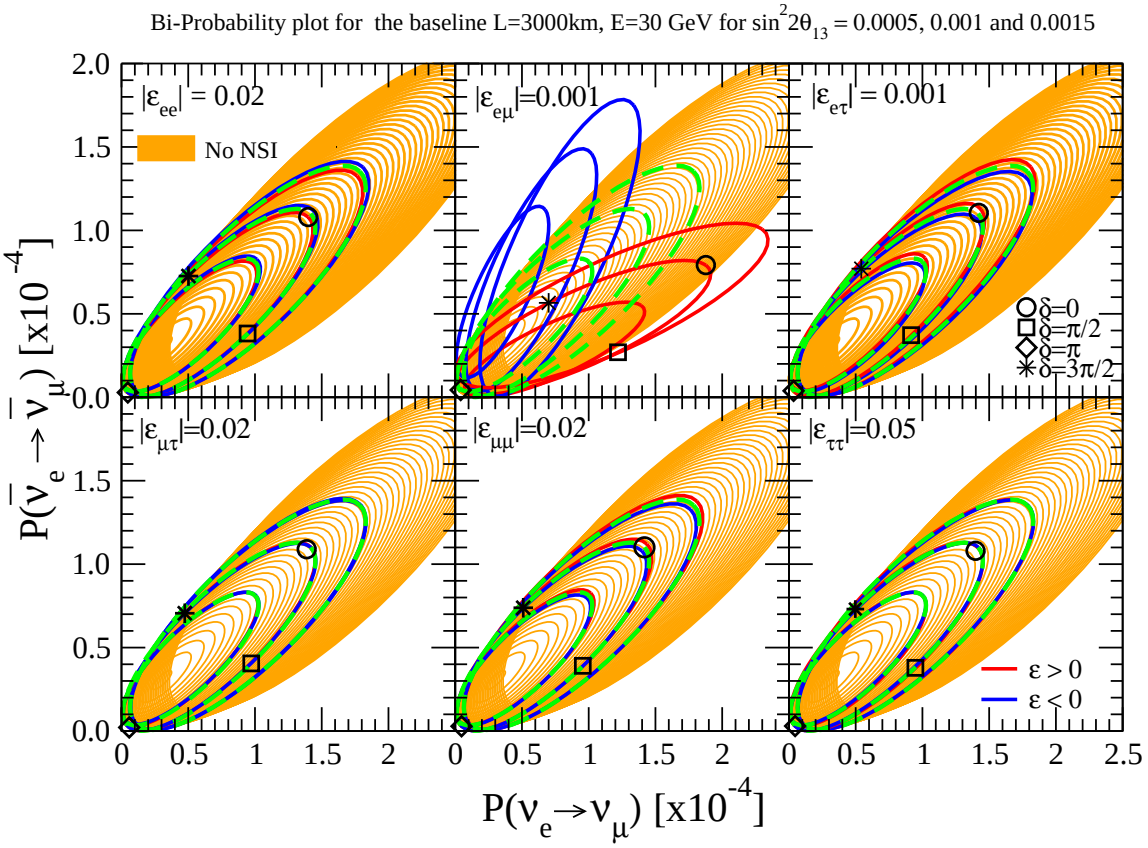

Figure 2: The same as in figure 1 but for the baseline $L = 3000$ km with the matter density $\rho = 3.6$ g/cm^3. The same values of ε are used in each panel. In the left and right lower panels the ellipses with positive and negative sign of ε overlap almost completely and each individual curve is not visible. The green ellipses which correspond to the same three values of $\sin^2 2\theta_{13}$ but without NSI are clearly visible.

well as ε_{ee} corresponding to the ones derived by Cervera *et al.* [28] for the standard case without ε. At the magic baseline, $\frac{aL}{4E} = \pi$, the formulas for the ν_μ appearance oscillation probability greatly simplifies. With NSI represented by $\varepsilon_{e\tau}$ it is given by

$$P(\nu_e \to \nu_\mu; \varepsilon_{e\tau}) = 4\frac{(\Delta m^2_{31})^2}{(a-\Delta m^2_{31})^2} s^2_{23} s^2_{13} \sin^2\left(\frac{\Delta m^2_{31} L}{4E}\right) \qquad (3.2)$$
$$+\frac{4ac_{23}s^2_{23}}{(a-\Delta m^2_{31})^2}\left[2\Delta m^2_{31} s_{13}|\varepsilon_{e\tau}|\cos(\delta+\phi_{e\tau})+c_{23}a|\varepsilon_{e\tau}|^2\right]\sin^2\left(\frac{\Delta m^2_{31} L}{4E}\right).$$

The corresponding formula for anti-neutrinos can be obtained by making the replacement $a \to -a$, $\delta \to -\delta$, and $\phi_{e\tau} \to -\phi_{e\tau}$. The formula with $\varepsilon_{e\mu}$ is very similar to (3.2). It is obtained by replacing $c_{23}\varepsilon_{e\tau}$ by $s_{23}\varepsilon_{e\mu}$ in the second line of eq. (3.2). Then, the value of $P(\nu_e \to \nu_\mu)$ with $\varepsilon_{e\tau}$ and $\varepsilon_{e\mu}$ are numerically equal with the values of the parameters used in figure 1, the maximal value of θ_{23} and $|\varepsilon_{e\tau}| = |\varepsilon_{e\mu}|$. It explains the identical behavior of the probabilities with $\varepsilon_{e\mu}$ and $\varepsilon_{e\tau}$ seen in the second and the third upper panels in figure 1. The ellipse in these panels shrink approximately to a line because there is only $\cos(\delta + \phi_{e\tau})$

dependence in the probability where $\phi_{e\tau}$ denotes the phase of $\varepsilon_{e\tau}$. The form $\cos(\delta + \phi_{e\tau})$ means that the shape and the location of shrunk ellipses in figure 1 are unchanged even when $\phi_{e\tau}$ is varied. The label of δ on the ellipse (if it is placed), of course, changes.

The length of the shrunk ellipse is equal to twice the coefficient of $\cos(\delta + \phi_{e\tau})$ of the last term in eq. (3.2). With the values of the parameters used (E=30 GeV, L = 7200 km, $\rho = 4.5$ g/cm^3, $\varepsilon_{e\tau} = 0.001$, $\sin^2 2\theta_{13} = 0.001$) it can be estimated as 1.8×10^{-5}, which is in perfect agreement with the length of the shrunk middle ellipse projected onto $P(\nu_e \to \nu_\mu)$ axis in figure 1. Therefore, we have understood the qualitative features of the flat ellipse at the magic baseline as well as its size.

We can also understand the reason why the effect of $\varepsilon_{\tau\tau}$ and $\varepsilon_{\mu\tau}$ are suppressed by deriving a similar formula which contains one of them in an analogous way as in appendix A. The leading order terms which involve one of these ε's are of order ϵ^3 and hence smaller.

3.2 Detector at $L = 3000$ km and the synergy expected when combined with the one at $L \simeq 7000$ km

It is instructive to compare the similar plot for the intermediate detector at $L = 3000$ km which is shown in figure 2 to figure 1 at $L = 7200$ km. The same values of ε's as in each corresponding panel in figure 1 are used. The three representative values of $\sin^2 2\theta_{13}$ used are also the same as in figure 1. We immediately notice several clear differences. First of all, the effect of δ is large at $L = 3000$ km for both cases with and without NSI, as indicated by the blue and the red lines (with NSI) and by the green ellipses as well as by wide span of the ellipses indicated by the orange region (without NSI). The ellipses with NSI, except for the case with $\varepsilon_{e\mu}$, are buried into this region. This is clearly the cause of the problem of confusion between θ_{13} and ε's one encounters when one tries to measure θ_{13} and δ allowing for NSI; The system with ε's can mimic the one with different values of θ_{13} but without NSI. In figure 2 the difference between the confused parameters and the genuine ones are small, apart from the $\varepsilon_{e\mu}$ case, because we take small values of ε's. It is also notable that the effect of the sign of the ε's is not quite visible, which is nothing but a consequence of the two-phase degeneracy as explained in section 2.2. (See section 6.2 for more about the degeneracy.)

When we try to determine the values of ε's it is also a bad news because there can be a severe confusion between NSI and the standard oscillation effect with θ_{13} and δ. We will see in sections 5 and 6 that this confusion for ε determination is much severer than that in $\theta_{13} - \delta$ determination at $L = 3000$ km, which will be manifested as a complicated island structure in the allowed region. On the other hand, when we try to measure θ_{13} and δ at $L = 3000$ km confusion due to the presence of ε's is not so significant *provided that the ε is small* as we see in figure 2. In particular, as we will see, the sensitivity to δ is good even after marginalization of ε's. (See figure 7–10 in section 5.)

On the other hand, at $L \simeq 7000$ km the sensitivity to ε's is great though essentially there is no sensitivity to δ. These consideration naturally suggest the possibility of combining the intermediate and the far detectors to determine simultaneously NSI parameters at the same time measuring θ_{13} and δ.

The markedly different behavior of the bi-probability plots between the $\varepsilon_{e\mu}$ and $\varepsilon_{e\tau}$ systems at $L \simeq 3000$ km can be traced back to the difference between the third terms in the analytic formulas (A.25) and (A.27). We should note that the almost identical behavior between the systems with $\varepsilon_{e\mu}$ and $\varepsilon_{e\tau}$ at $L = 7000$ km, and the marked difference between them at $L \simeq 3000$ km makes it interesting by itself to compare their sensitivities at these two baselines and when they are combined. We will see later that sensitivity to $\varepsilon_{e\mu}$ is essentially determined by the effect at $L = 3000$ km whereas that to $\varepsilon_{e\mu}$ is determined by the combination of $L = 3000$ km and 7000 km.

4. Analysis method

4.1 Assumptions

In our analysis in this paper, we make the following assumptions for the parameters of neutrino factory. We assume an intense muon storage ring which can deliver 10^{21} useful decaying muons per year. The muon energy is taken to be 50 GeV. We assume 4 years running in neutrino and 4 years running in anti-neutrino modes, respectively. We assume the two magnetized iron detectors, one at baseline $L = 3000$ km and the other at $L = 7000$ km which is close to but not exactly the magic baseline $L_{\rm magic}$.[1] Each detector is assumed to have fiducial mass of 50 kton. We consider the golden channels, $\nu_e \to \nu_\mu$ and $\bar{\nu}_e \to \bar{\nu}_\mu$ in this paper. For simplicity, we use the constant matter density approximation throughout this work, and take the Earth matter density along the neutrino trajectory as $\rho = 3.6$ g/cm^3 and $\rho = 4.5$ g/cm^3 for baselines $L = 3000$ km and at $L = 7000$ km, respectively. The electron fraction Y_e is assumed to be 0.5. We believe that using more realistic Earth matter density profile will not change much our results.

In most part of our analysis we make the following simplifications: (1) We ignore all the background due to the misidentification of muon charges and other causes. (2) We neglect the systematic uncertainties. Since the muon detection at high energies is supposed to be extremely clean in magnetized iron detectors the simplification (1) may not affect the results in a significant way apart from the case of extremely small θ_{13}. With regard to the systematic errors we feel that no solid numbers are known yet in spite of the fact that great amount of efforts are made toward reliable estimation of them [44]. Nevertheless, we will try to estimate to what extent the sensitivities we obtain in our analysis are affected by introduction of background and the systematic errors. See section 5.5.

We always take the normal mass hierarchy as an input. We will consider in this paper various cases in which only two different flavor elements of NSI ($\varepsilon_{\alpha\beta}$) are turned on at the

[1] By assuming the far detector at baseline somewhat off $L_{\rm magic}$, we want to demonstrate that it is not quite necessary to place it exactly at $L_{\rm magic}$. First of all, we feel it unrealistic that one can place the far detector at $L_{\rm magic}$ with a mathematical precision. Apart from the problem of site availability, the exact magic baseline cannot be determined prior measurement unless the values of the relevant mixing parameters, the earth matter density along the neutrino trajectory and its relationship with the effective density for neutrino oscillation [42] are precisely known. Only a posteriori the matter density can be measured in situ in the experiment [41].

JHEP12(2007)002

same time. We also assume that $\varepsilon_{\alpha\beta}$ is real, leaving the interesting topics of complex phase effects to elsewhere.

4.2 Analysis procedure

We define the χ^2 function as follows,

$$\chi^2 \equiv \min_{\theta_{13},\delta,\varepsilon} \sum_{i=1}^{3}\sum_{j=1}^{2}\sum_{k=1}^{2} \frac{\left[N_{i,j,k}^{\rm obs} - N_{i,j,k}^{\rm theo}(\theta_{13},\delta,\varepsilon)\right]^2}{N_{i,j,k}^{\rm theo}(\theta_{13},\delta,\varepsilon)}, \tag{4.1}$$

where $N_{i,j,k}^{\rm obs}$ is the number of observed (simulated) events computed by using the given input parameters and $N_{i,j,k}^{\rm theo}$ is the theoretically expected number of events to be varied in the fit by freely varying the mixing and NSI parameters. Since we ignore the systematic uncertainties, the denominator in (4.1) represent the statistical uncertainties. The summation with respect to indices i, j and k imply energy (3 bins), baseline (3000 km or 7000 km), and the type of neutrinos (neutrino or anti-neutrino), respectively. The intervals of 3 energy bins we consider are 4-8 GeV, 8-20 GeV and 20-50 GeV for neutrinos and 4-15 GeV, 15-25 GeV and 25-50 GeV for anti-neutrinos.

The theoretically expected number of events are computed as

$$N^{\rm theo}(\theta_{13},\delta,\varepsilon) = n_\mu T M \frac{10^9 N_{\rm A}}{m_\mu^2 \pi}\frac{E_\mu^2}{L^2}\int_{E_{\rm min}}^{E_{\rm max}} g(E)\,\sigma_{\nu_\mu(\bar\nu_\mu)}(E)\,P_{\nu_e\to\nu_\mu(\bar\nu_e\to\bar\nu_\mu)}(E;\theta_{13},\delta,\varepsilon)dE, \tag{4.2}$$

where n_μ is the number of useful muon decays per year, T is the exposure period (in years), M is the detector mass (in ktons), N_A is the Avogadro's number, m_μ is the muon mass, E_μ is the energy of the stored muons, L is the baseline, $\sigma_{\nu_\mu(\bar\nu_\mu)}(E)$ is the charged current interaction cross section for ν_μ and $\bar\nu_\mu$, and $P_{\nu_e\to\nu_\mu(\bar\nu_e\to\bar\nu_\mu)}(E;\theta_{13},\delta,\varepsilon)$ is the oscillation probability. In this work, we considered the case where $E_\mu = 50\,$GeV, $M = 50$ kton, $T = 4$ yr for both neutrinos and anti-neutrinos, and $n_\mu = 10^{21}$ per year. The function $g(E)$ which is given as

$$g(E) \equiv 12\frac{E^2}{E_\mu^3}\left(1 - \frac{E}{E_\mu}\right) \tag{4.3}$$

is the unoscillated ν_e or $\bar\nu_e$ energy spectrum normalized to 1.

We assume, for simplicity, the detection efficiency is 100%.[2] We neglect the finite energy resolution in the detectors. Since the number of energy bins are small (=3) inclusion of the energy resolution will not alter the results in a significant way.

The observed number of events are computed exactly in the same way but using the given input parameters of θ_{13}, δ and NSI parameters (ε), so that $\chi^2_{\rm min} = 0$ at the best fit point by construction.

Using the χ^2 function defined in eq. (4.1), we define the allowed (sensitivity) regions by the commonly used condition, $\Delta\chi^2 \equiv \chi^2 - \chi^2_{\rm min} = 2.3$, 6.18 and 11.83 for 1, 2 and 3 σ confidence level (CL) for 2 degrees of freedom (DOF), unless otherwise stated.

[2] If the efficiency is $f\times 100\%$ we are effectively assuming the fiducial mass of the detector of $50/f$ kton. In the current estimate f is expected to be about 0.8 apart from an extremely low energy region $\sim 5\,$GeV [44].

5. Sensitivity to non-standard interactions and measurement of θ_{13} and δ with NSI

In this section, we discuss the sensitivity to NSI by the two detector setting. We also discuss the accuracy of the determination of the mixing parameters θ_{13} and δ in the presence of NSI. For these purposes we take the input values of two ε's to be zero (or equivalently vanishingly small) but freely vary them in fitting the data. The case with non-zero input values of ε's will be dealt with in section 6. To demonstrate the synergy between the intermediate and the far detectors we present the sensitivity to NSI for each detector as well as the combined one throughout this and the next sections. As a typical value of θ_{13} we consider the case of $\sin^2 2\theta_{13} = 10^{-3}$, though we also discuss the case with $\sin^2 2\theta_{13} = 10^{-4}$ to show how the sensitivities depend on θ_{13}. We have examined the four values of δ, $\pi/4$, $\pi/2$, π, and $3\pi/2$ as representative cases. However, we present only part of the figures we have drawn not to make this paper too long.

5.1 Constraining NSI; case of zero input

In figures 3–6, we present the constraint on NSI that can be imposed by the neutrino factory measurement defined in section 4.1 with various selected combination of two ε parameters.[3] Figure 3 and 4 are for $\delta = \pi/4$ whereas figure 5 and 6 are for $\delta = 3\pi/2$. The left, the middle, and the right panels of figures 3 and 5 (figures 4 and 6) are for the combination, showing horizontal - vertical axes, $\varepsilon_{ee}-\varepsilon_{e\tau}$, $\varepsilon_{\tau\tau}-\varepsilon_{e\tau}$, $\varepsilon_{ee}-\varepsilon_{\tau\tau}$ ($\varepsilon_{ee}-\varepsilon_{e\mu}$, $\varepsilon_{\tau\tau}-\varepsilon_{e\mu}$, $\varepsilon_{e\tau}-\varepsilon_{e\mu}$), respectively. The top, the middle, and the bottom panels are, respectively, for the baselines $L = 3000$ km, $L = 7000$ km, and the two baselines combined. The blue, the red, and the green curves are the allowed contours at 1σ, 2σ and 3σ CL for 2 DOF, respectively.

We observe that from the results presented in figure 3 through figure 6, the detector at $L = 3000$ km alone does not have good resolution power for the possible existence of ε's, except for $\varepsilon_{e\mu}$. The parameter $\varepsilon_{e\mu}$ is special since its impact on the oscillation probability is so large (as seen in figure 2) that the measurement at $L = 3000$ km alone can give a strong constraint on $\varepsilon_{e\mu}$ which seems consistent with the result obtained in ref. [25]. Apart from the cases which involve $\varepsilon_{e\mu}$, the effect of the simultaneous presence of two ε's is manifest in the appearance of many correlated regions/islands, though the precise shapes of the regions depend on which combination of ε's is turned on and on which input value of δ is used.

A similar statement applies to the case of the detector at L=7000 km. But, the correlation between ε's is quasi one-dimensional for most of the combinations though we see branch structure in $\varepsilon_{ee} - \varepsilon_{e\tau}$ case and sizable width in the $\varepsilon_{\tau\tau} - \varepsilon_{e\tau}$ case. Overall, the constraints on the diagonal elements, ε_{ee} and $\varepsilon_{\tau\tau}$, are much looser compared to those on $\varepsilon_{e\tau}$ and $\varepsilon_{e\mu}$. The latter feature comes from high sensitivities to the off-diagonal ε's expected at the magic baseline as discussed in section 3.1, while less sensitivity to the former is expected by figures 1 and 2. The feature of correlation is least obvious in the combination $\varepsilon_{ee}-\varepsilon_{\tau\tau}$ though indicating a weak oblique linear dependence. For the branch-like structure

[3] It appears to us that ragged behavior of the contours seen in some of the plots is of physical origin due to the complicated structure of four-dimensional χ^2 function. Some of the structures, however, could be smoothen to a certain extent by introducing a finer grid and the finite energy resolution.

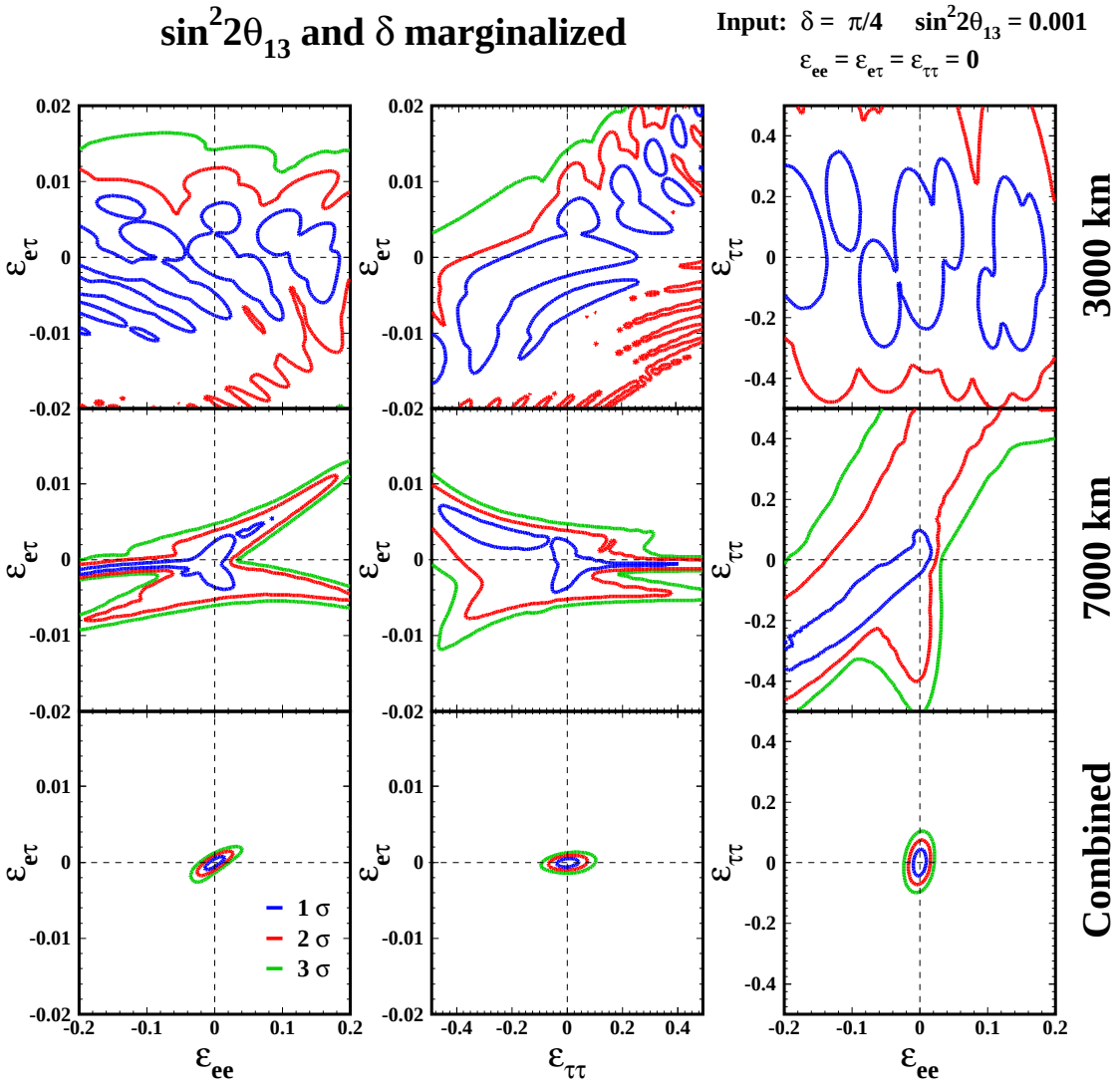

Figure 3: Allowed regions projected into the plane of 2 NSI parameters, ε_{ee}-$\varepsilon_{e\tau}$ (left panels), $\varepsilon_{\tau\tau}$-$\varepsilon_{e\tau}$ (middle panels) and ε_{ee}-$\varepsilon_{\tau\tau}$ (right panels) corresponding to the case where the input parameters are $\sin^2 2\theta_{13} = 0.001$ and $\delta = \pi/4$ and no non-standard interactions (or all the ε's are zero), for $E_\mu = 50\,\text{GeV}$ and the baseline of $L = 3000$ km (upper panels), 7000 km (middle horizontal panels) and combination (lower panels). The thin dashed lines are to indicate the input values of $\varepsilon_{\alpha\beta}$. The fit was performed by varying freely 4 parameters, θ_{13}, δ and 2 ε's with θ_{13} and δ being marginalized. The number of muons decays per year is 10^{21}, the exposure considered is 4 (4) years for neutrino (anti-neutrino), and each detector mass is assumed to be 50 kton. The number of energy bins considered is three. The other standard oscillation parameters are fixed as $\Delta m^2_{23} = 2.5 \times 10^{-3}\,\text{eV}^2$, $\sin^2\theta_{23} = 0.5$, $\Delta m^2_{12} = 8.0 \times 10^{-5}\,\text{eV}^2$ and $\sin^2\theta_{12} = 0.31$.

we will make comments to clarify its nature in section 6 because the structure is even more prominent with non-zero ε input.

JHEP12(2007)002

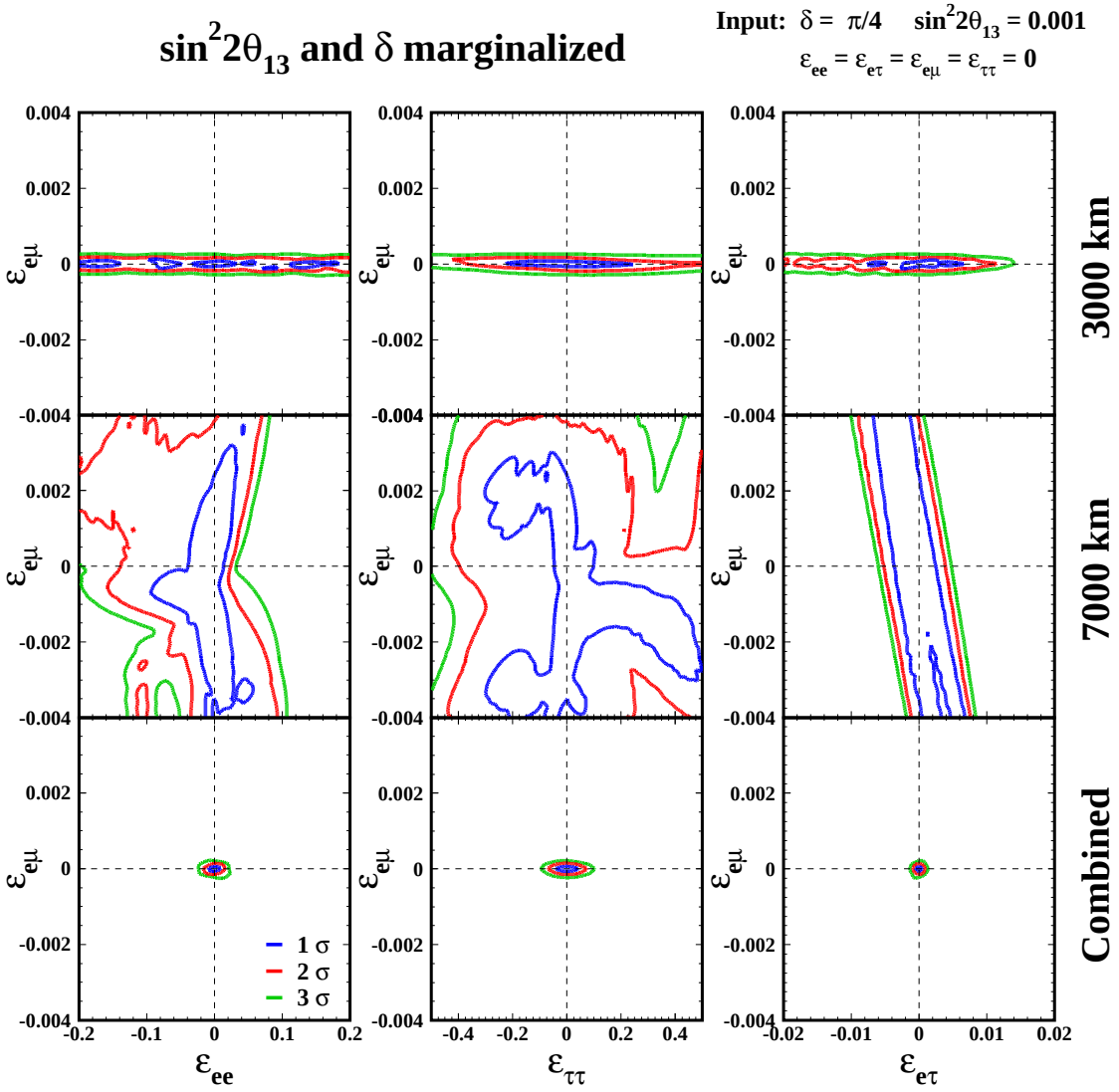

Figure 4: The same as in figure 3 but for a different combination of 2 ε's, ε_{ee}-$\varepsilon_{e\mu}$ (left panels), $\varepsilon_{\tau\tau}$-$\varepsilon_{e\mu}$ (middle panels) and $\varepsilon_{e\mu}$-$\varepsilon_{e\tau}$ (right panels).

The effect of combining the intermediate and the far detectors is remarkable. The allowed regions scattered in wide ranges in the top (3000 km) and the middle (7000 km) panels combine into a much smaller region in the bottom panel in figures 3–6. We should remark that although the above mentioned over-all features remain unchanged for different values of δ, the resultant sensitivity to ε's depends rather strongly on the value of CP phase δ as one can see by comparing between figure 3 and figure 5. The problem of δ dependence of the sensitivity to ε's will be fully addressed in section 7.

One may ask the question why the scattered regions in the top panel and the extended region in the middle panel in each column in figure 3 and figure 5, and figure 4 and

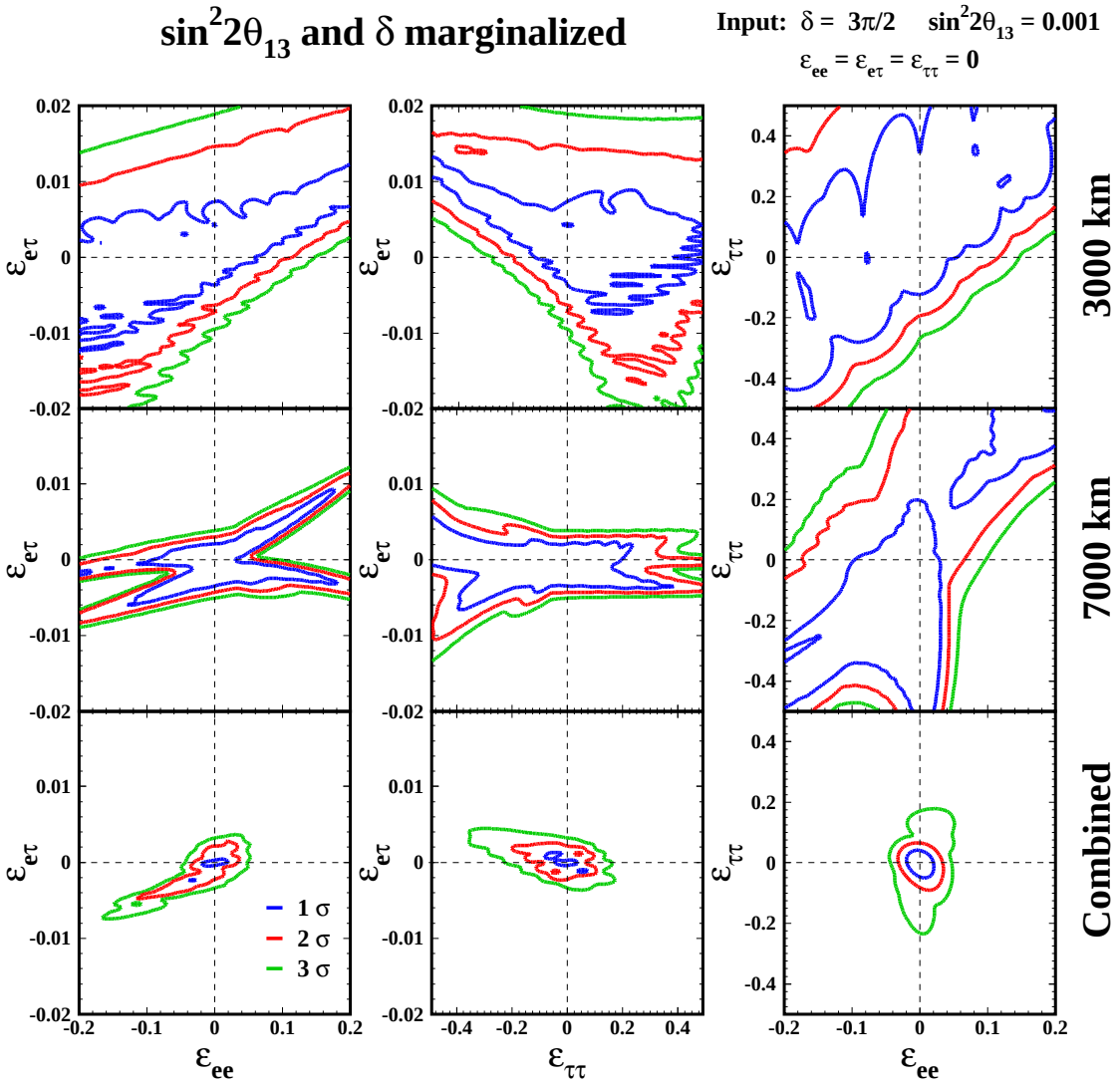

Figure 5: The same as in figure 3 but with $\delta = 3\pi/2$.

figure 6, can be combined to yield such a small region. The answer is that it is due to the CP phase δ. Namely, most of the region of overlap between the top and the middle panels have mismatch in value of δ, and hence they do not survive when the two constraints are combined. Therefore, keeping the solar Δm^2 and the KM phase degree of freedom is the key to the high sensitivity to ε's we observe in figures 3–6. The synergy effect that merit us by combining the intermediate and the far detectors are even more significant compared with the one in identical two detector method for measuring CP violation and determining the mass hierarchy [45, 46].

Our last comment in this subsection is that a characteristic feature that manifest itself in figures 3–6 gives us a warning. Namely, one could significantly overestimate the

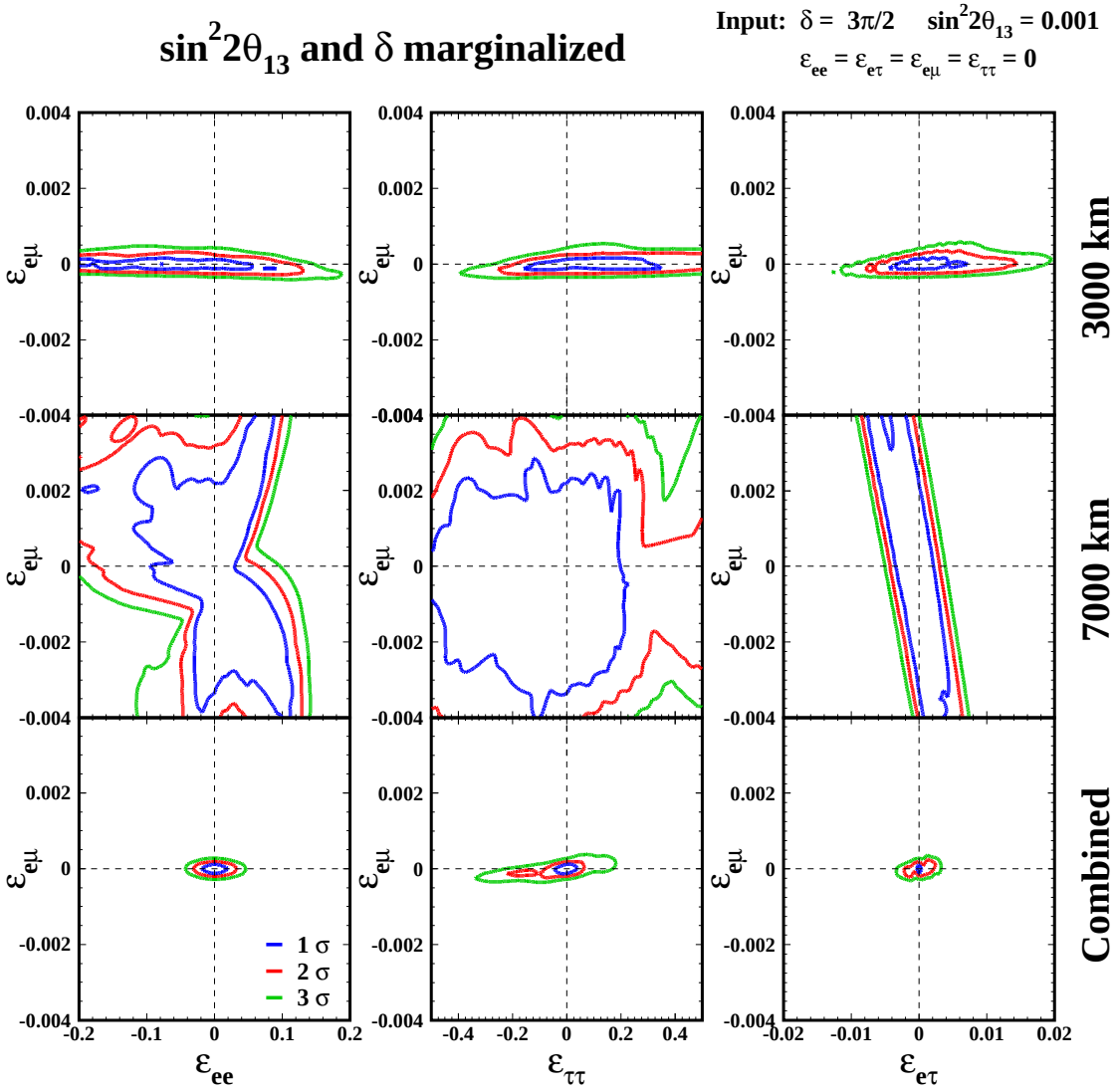

Figure 6: The same as in figure 4 but with $\delta = 3\pi/2$.

sensitivity to detection of non-vanishing NSI by working only with a particular single element ε_{ee} or $\varepsilon_{e\tau}$, for example. By working with two ε's at the same time one is able to recognize the whole structure as given in these figures.[4]

5.2 Sensitivity to θ_{13} and δ in the presence of NSI; case of zero input

We now examine the sensitivities to θ_{13} and δ in the presence of NSI. In figure 7 through figure 10 we present the sensitivities to θ_{13} and δ by taking the same input value of θ_{13},

[4]It also raises the question whether the two ε systems are sufficiently generic to reveal the full structure of the systems with larger number of ε's which have a multi-dimensional χ^2 manifold. We are not able to answer the question in this paper.

$\sin^2 2\theta_{13} = 10^{-3}$. Figures 7 and 8 are for $\delta = \pi/4$, whereas figures 9 and 10 are $\delta = 3\pi/2$. The organization of the figures is the same as in figures 3–6.

Let us look at the top panel for the detector at $L = 3000$ km. We clearly observe the phenomenon of "confusion" in the presence of NSI, in particular for the case of $\delta = 3\pi/2$. Namely, NSI can mimic the effect of non-zero θ_{13} so that the allowed region extends to a very small value of θ_{13}. However, this feature is strongly perturbed by the measurement at $L = 7000$ km. Because it is highly sensitive to the effects of NSI, it helps to resolve the confusion between NSI and θ_{13}. After combining informations of the intermediate and the far detectors a tiny region in $\sin^2 2\theta_{13} - \delta$ space results, as one can observe in the bottom panels in figure 7 through figure 10. Thus, the problem of NSI - θ_{13} confusion can be solved by the two detector setting.[5]

5.3 How do the sensitivities depend on θ_{13}?

We discuss briefly how the sensitivities change when we take a smaller value of θ_{13}, for example, $\sin^2 2\theta_{13} = 0.0001$. We present our results only for $\delta = 3\pi/2$ for reasons of limitation of space but make some comments on the other cases. In figures 11 and 12 we show the sensitivities to NSI parameters which may be compared to the corresponding figures, figures 5 and 6, for the case $\sin^2 2\theta_{13} = 0.001$. To our surprise, the over-all features of the allowed regions are similar between the two cases. The only notable changes are that: (1) in the $\varepsilon_{ee} - \varepsilon_{\tau\tau}$ system the sensitivities to these ε's becomes worse by a factor of 3-4, but (2) in all the three systems which involve $\varepsilon_{e\mu}$, $\varepsilon_{ee} - \varepsilon_{e\mu}$, $\varepsilon_{\tau\tau} - \varepsilon_{e\mu}$, and $\varepsilon_{e\tau} - \varepsilon_{e\mu}$, the sensitivities become *better* for $\sin^2 2\theta_{13} = 0.0001$. The similar worsening or improvement of the sensitivities to NSI are observed in other values of δ. They become worse in some cases, in particular, in the $\varepsilon_{ee} - \varepsilon_{\tau\tau}$ system with $\delta = \pi/4$ and $\pi/2$ at $L = 3000$ km. The sensitivities to ε_{ee} and $\varepsilon_{\tau\tau}$ improve by almost a factor of 2 at $\delta = \pi$ with $\sin^2 2\theta_{13} = 0.0001$ compared to the case of 0.001. The sensitivity to $\varepsilon_{e\tau}$ gets improved by about a factor of 2 in the $\varepsilon_{e\mu} - \varepsilon_{e\tau}$ system at $\delta = \pi/4$. Thus, most of the improvement occur in the systems which involve $\varepsilon_{e\mu}$. The reason is that the sensitivity to $\varepsilon_{e\mu}$ is particularly good at $L = 3000$ km and it makes the synergy effect even stronger.

We notice that the branch structure we saw in section 5.1 is also rounded off, and the island structure becomes less prominent at $\sin^2 2\theta_{13} = 0.0001$. The smoothing of the contour and the improvement of the sensitivity may be due to the fact that at such very small θ_{13} the effect of NSI becomes important compared to the standard oscillation effect.

On the other hand, the sensitivity to θ_{13} and δ definitely becomes worse when we go down to $\sin^2 2\theta_{13} = 0.0001$ as shown in figures 13 and 14. First of all, the problem of θ_{13}-NSI confusion becomes severer as one can see by comparing figures 13 and 14 to figures 9 and 10. A new allowed region emerges in the $\varepsilon_{ee} - \varepsilon_{e\tau}$ and $\varepsilon_{\tau\tau} - \varepsilon_{e\tau}$ systems at $L = 3000$ km. Due to lack of statistics at the small θ_{13} sensitivity to θ_{13} is significantly reduced at $L = 7000$ km, leading to the visible loss of the sensitivities.

[5]The "confusion theorem" stated in [14] refers to the situation in which we have both NSI at source and in propagation and they are related with each other in a specific way. Therefore, our discussion in this paper does not affect the validity of this theorem.

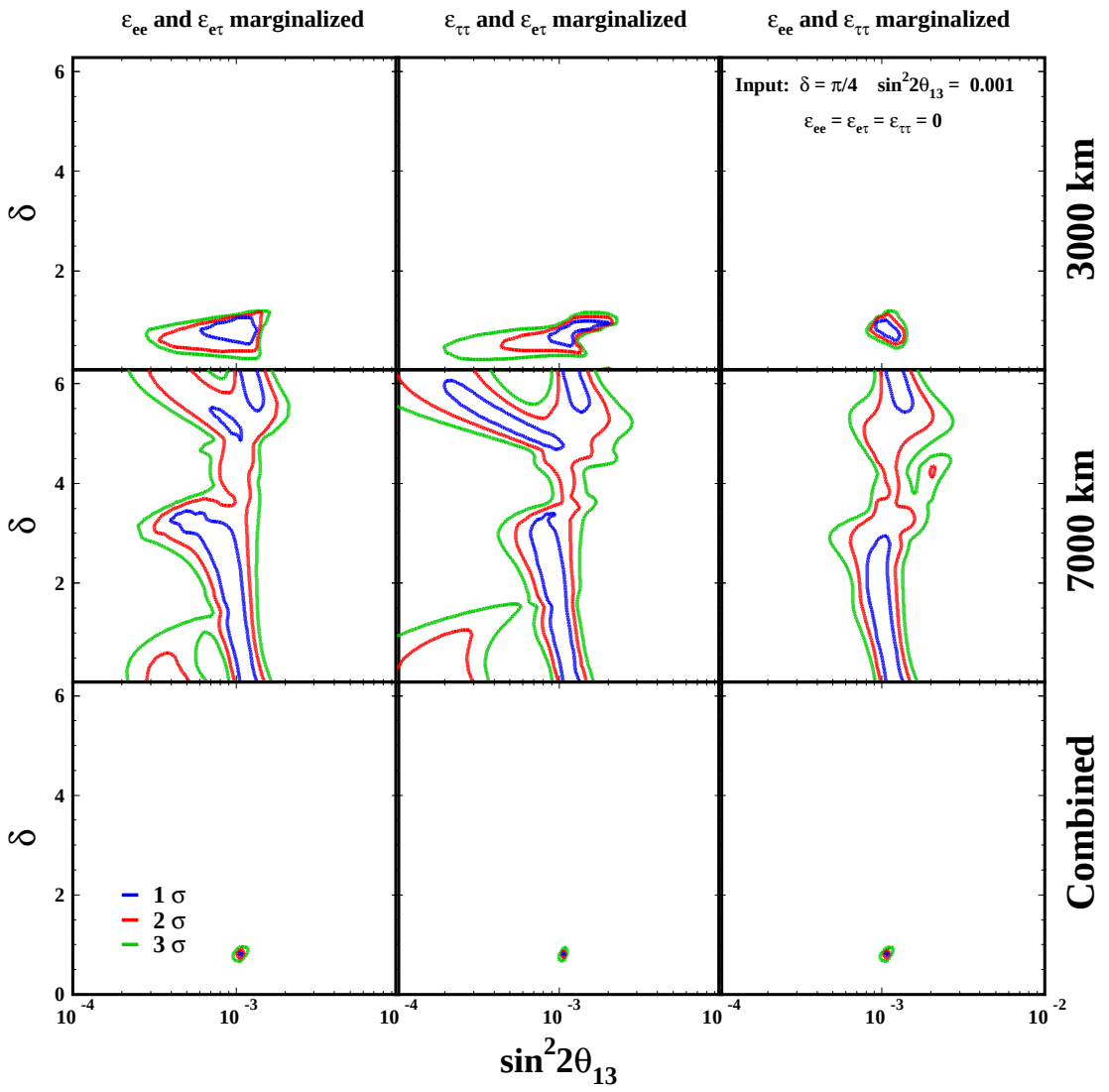

Figure 7: Allowed regions projected into the plane of $\sin^2 2\theta_{13}$-δ corresponding to the case where the input parameters are $\sin^2 2\theta_{13} = 0.001$ and $\delta = \pi/4$ and no non-standard interactions (or all the ε's are zero), for $E_\mu = 50\,\mathrm{GeV}$ and the baseline of $L = 3000$ km (upper panels), 7000 km (middle horizontal panels) and combination (lower panels). The fit was performed by varying freely 4 parameters, θ_{13}, δ and 2 ε's where $\varepsilon_{\mathrm{ee}}$ and $\varepsilon_{e\tau}$ are marginalized (left panels), $\varepsilon_{\tau\tau}$ and $\varepsilon_{e\tau}$ are marginalized (middle panels) and $\varepsilon_{\mathrm{ee}}$ and $\varepsilon_{\tau\tau}$ are marginalized (right panels). The same input and fitting parameters as in figure 3 but projections are made into the different parameter space.

In summary, neutrino factory with two detector setup at $L = 3000$ and 7000 km is more resistant to small values of θ_{13} as a discovery machine for NSI, rather than as a machine for precision measurement of θ_{13} and δ.

JHEP12(2007)002

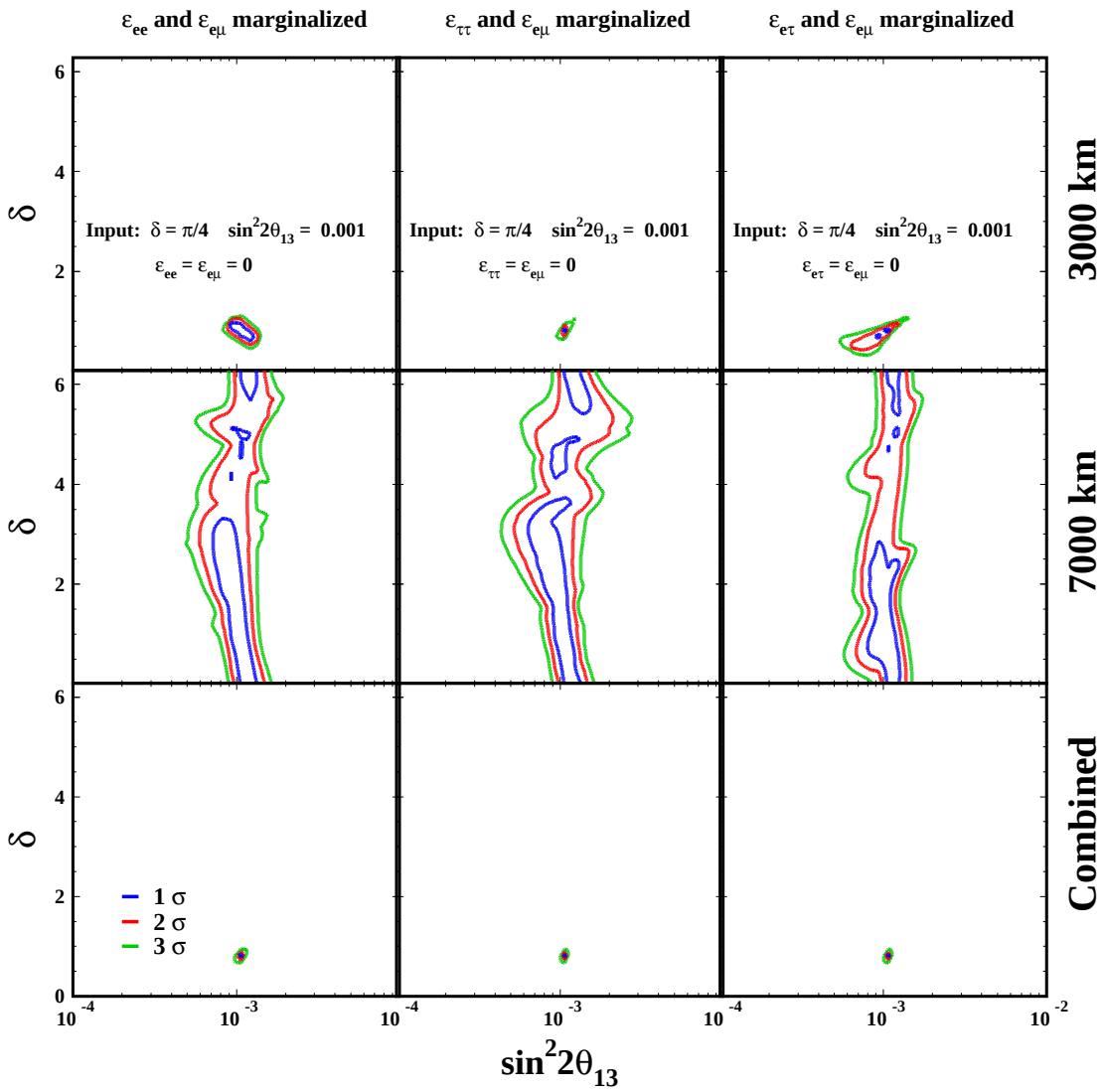

Figure 8: The same as in figure 7 but for different combination of 2 ε's to which the fit to $\sin^2 2\theta_{13}$ and δ is marginalized; $\varepsilon_{\rm ee}$-$\varepsilon_{e\mu}$ (left panels), $\varepsilon_{\tau\tau}$-$\varepsilon_{e\mu}$ (middle panels) and $\varepsilon_{e\mu}$-$\varepsilon_{e\tau}$ (right panels).

5.4 Comparing the sensitivities to θ_{13} and δ for cases with and without NSI

It may be worthwhile to compare the sensitivities to θ_{13} and δ for cases without NSI to the one with NSI using the same machinery used in our foregoing analysis. In figure 15 we present the results without NSI. The results are to be compared with those in figures 7–10. The resultant sensitivities to θ_{13} and δ are extremely good compared to those obtained for the cases with NSI. We will quantify this comparison in a more extensive way in section 7 where we will cover the whole space of interest in θ_{13} and δ.

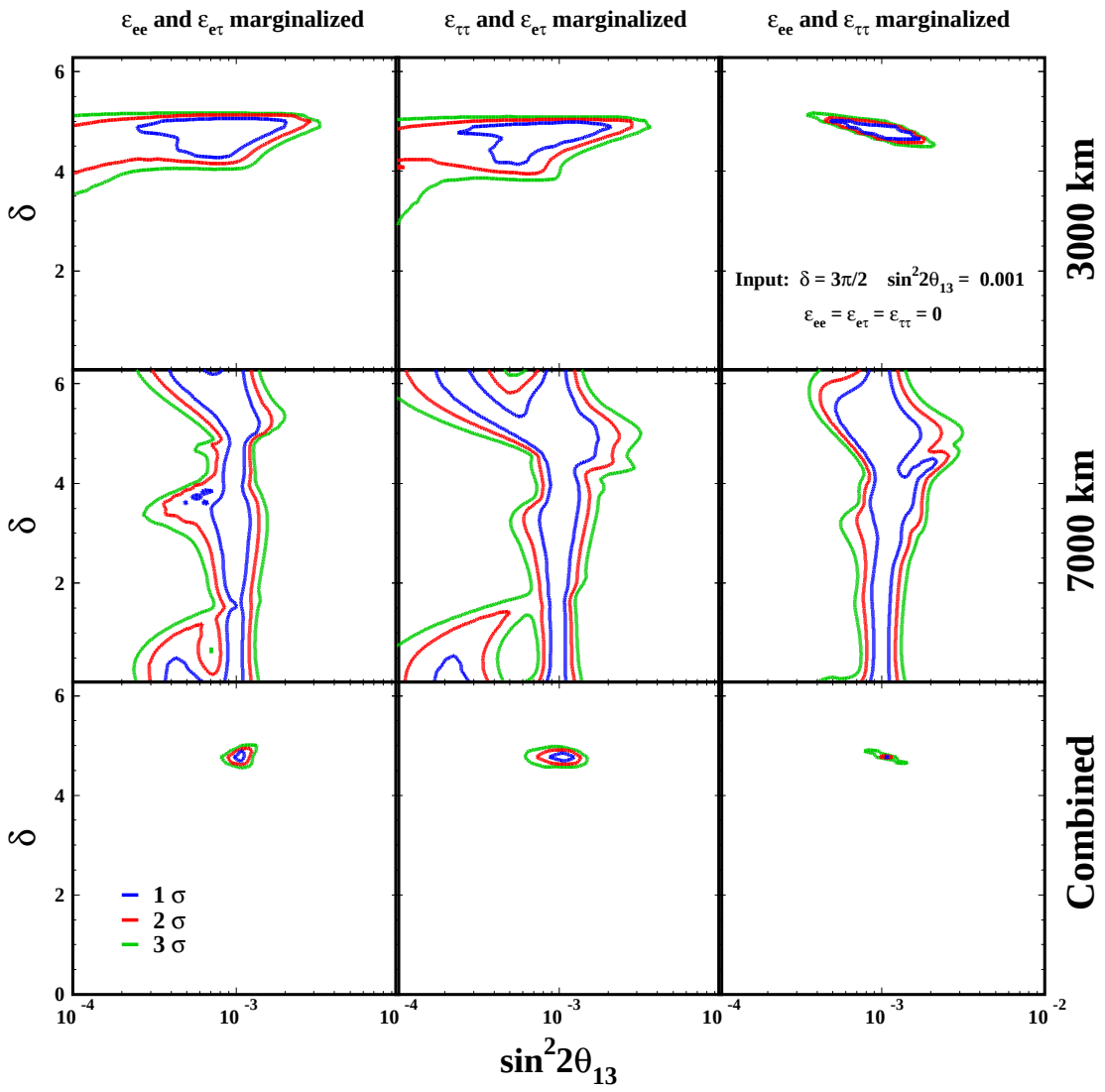

Figure 9: The same as in figure 7 but with $\delta = 3\pi/2$.

5.5 Effect of background and systematic errors

To have a rough idea of the possible effects of the background and the systematic uncertainties to the sensitivities we have repeated the computation with these effects at $\delta = \pi/4$ for various values of θ_{13} in ε_{ee}-$\varepsilon_{e\tau}$, $\varepsilon_{\tau\tau}$-$\varepsilon_{e\tau}$, and ε_{ee}-$\varepsilon_{\tau\tau}$ systems, which correspond to figure 3, figure 7, and $\delta = \pi/4$ counterpart of figure 11 (not shown). We estimate the number of background events by using the signal to noise ratio calculated in ref. [47], and rescaling the background to the number of useful muon decays used in this paper. We assign 20% uncertainty to the number of background events. We also take 2.5% as the total systematic uncertainty on the measurement.

For $\sin^2 2\theta_{13} = 0.001$, we find that the introduction of systematic uncertainties and

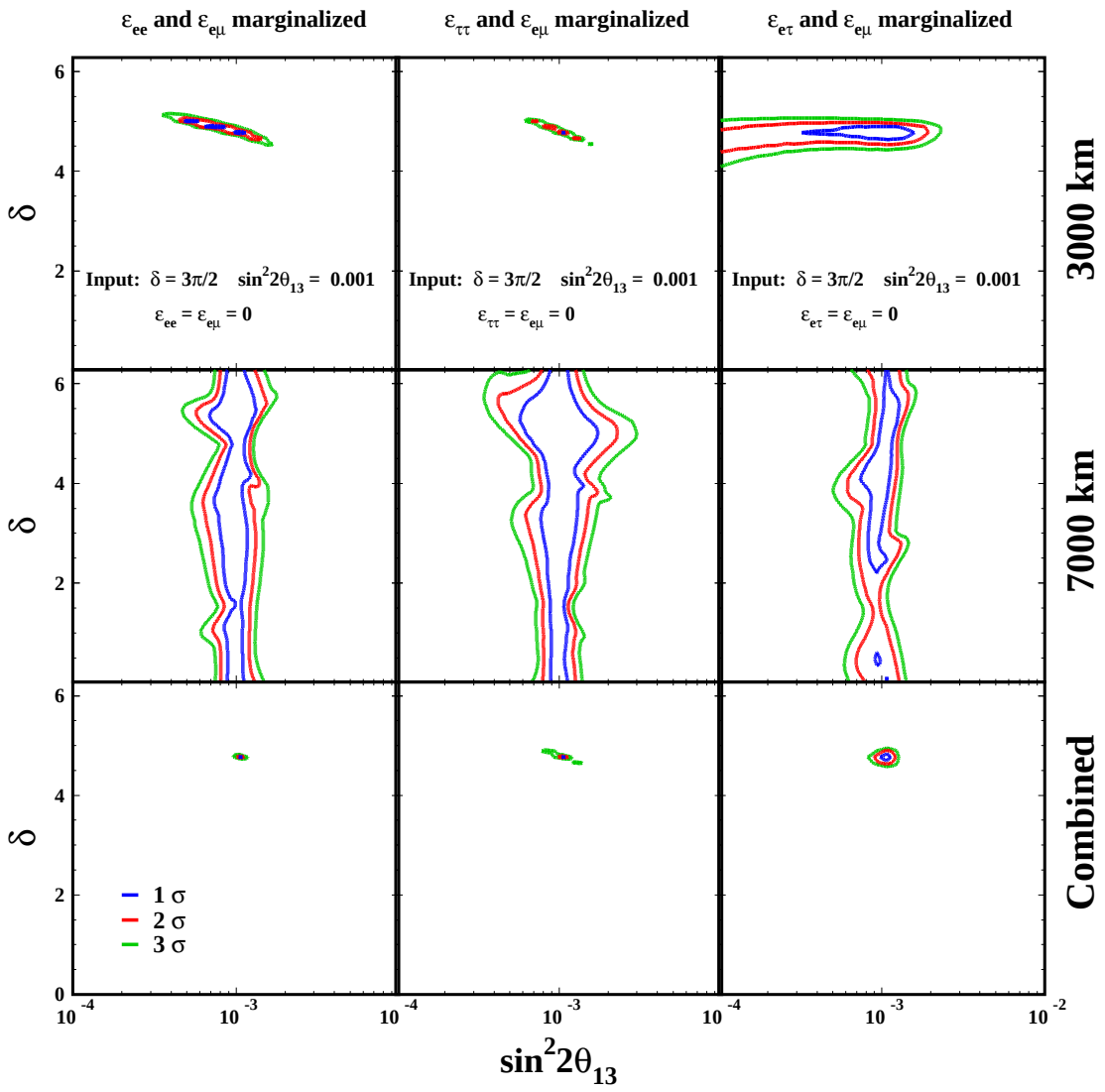

Figure 10: The same as in figure 8 but with $\delta = 3\pi/2$.

background lead to decrease in the sensitivity to $\varepsilon_{e\tau}$ by $\simeq 30\%$. The worsening of the sensitivity to $\varepsilon_{\rm ee}$ and $\varepsilon_{\tau\tau}$ depends upon the sub-system being within the ranges 30%-60% and 40%-50%, respectively. The effect of systematic errors and background is less prominent at $\sin^2 2\theta_{13} = 0.005$ but becomes larger at $\sin^2 2\theta_{13} = 0.0001$, making the sensitivity a factor of 2 worse.

On the other hand, the sensitivity to δ and $\sin^2 2\theta_{13}$ would be worsen by 30%-40% and 50%, respectivelly, at $\sin^2 2\theta_{13} = 0.001$, more or less independently of the sub-system treated and on the ε's discussed. An interesting feature of the sensitivity to δ and θ_{13} is that the effect of systematic errors diminishes as θ_{13} becomes small, and is at $\sim 20\%$ (30%) level for δ and $\sin^2 2\theta_{13}$, respectivelly, at $\sin^2 2\theta_{13} = 0.0001$. Therefore, the impact

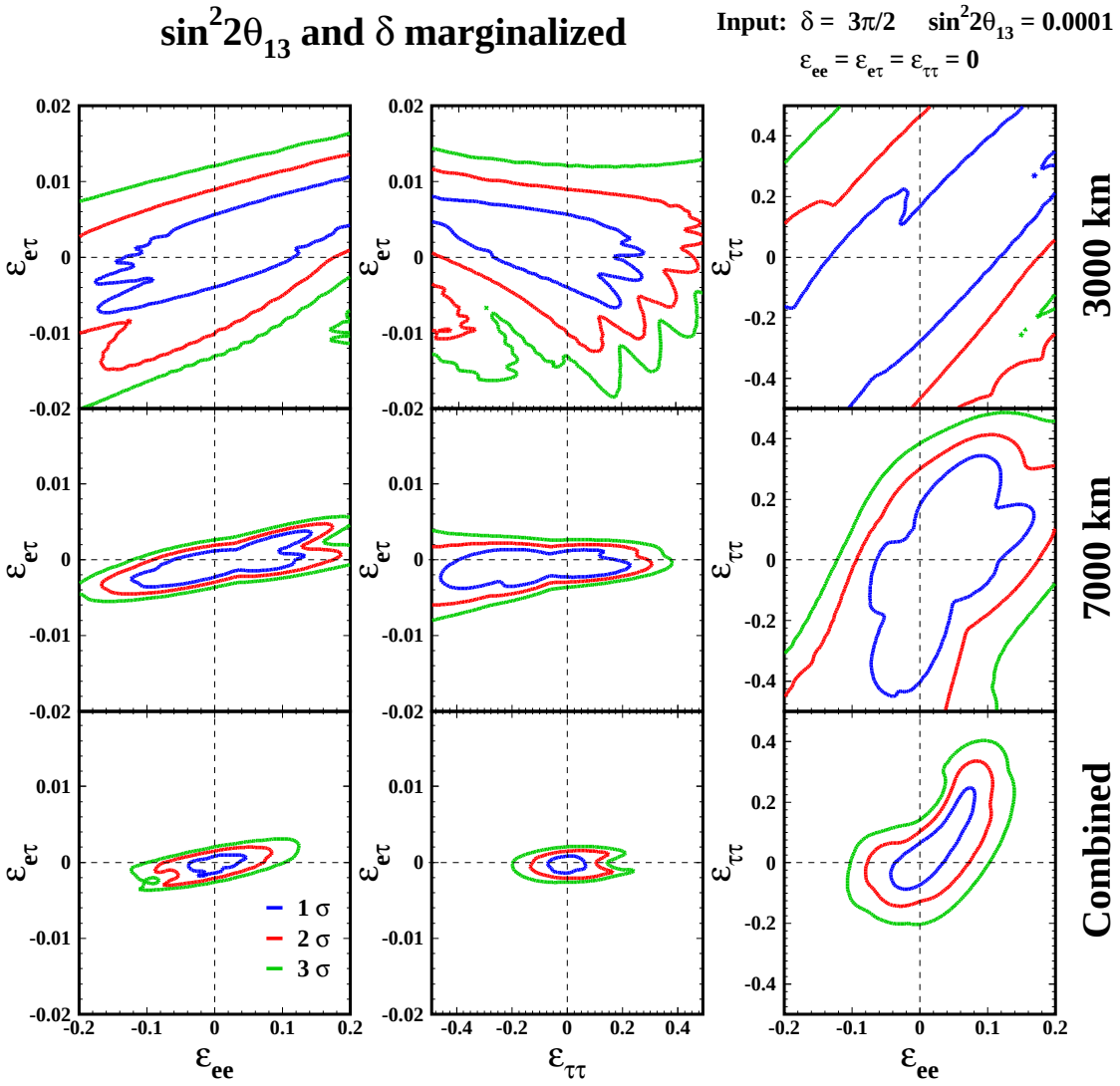

Figure 11: The same as in figure 5 but with $\sin^2 2\theta_{13} = 0.0001$.

of including the systematic to the sensitivity of δ and θ_{13} is limited in size, which *is* good news. All numbers were evaluated at 3 σ CL.

Though we continue to ignore the systematic uncertainties and the background in the rest of the analysis in this paper, the reader should remind that the estimated sensitivities to NSI, δ, and θ_{13} have uncertainties at the level quoted above. To completely remove the uncertainties requires precise knowledges of the performance of the detector.

6. Accuracies of determination of NSI, θ_{13}, and δ

We now discuss the question of how well the magnitude of non-vanishing NSI can be deter-

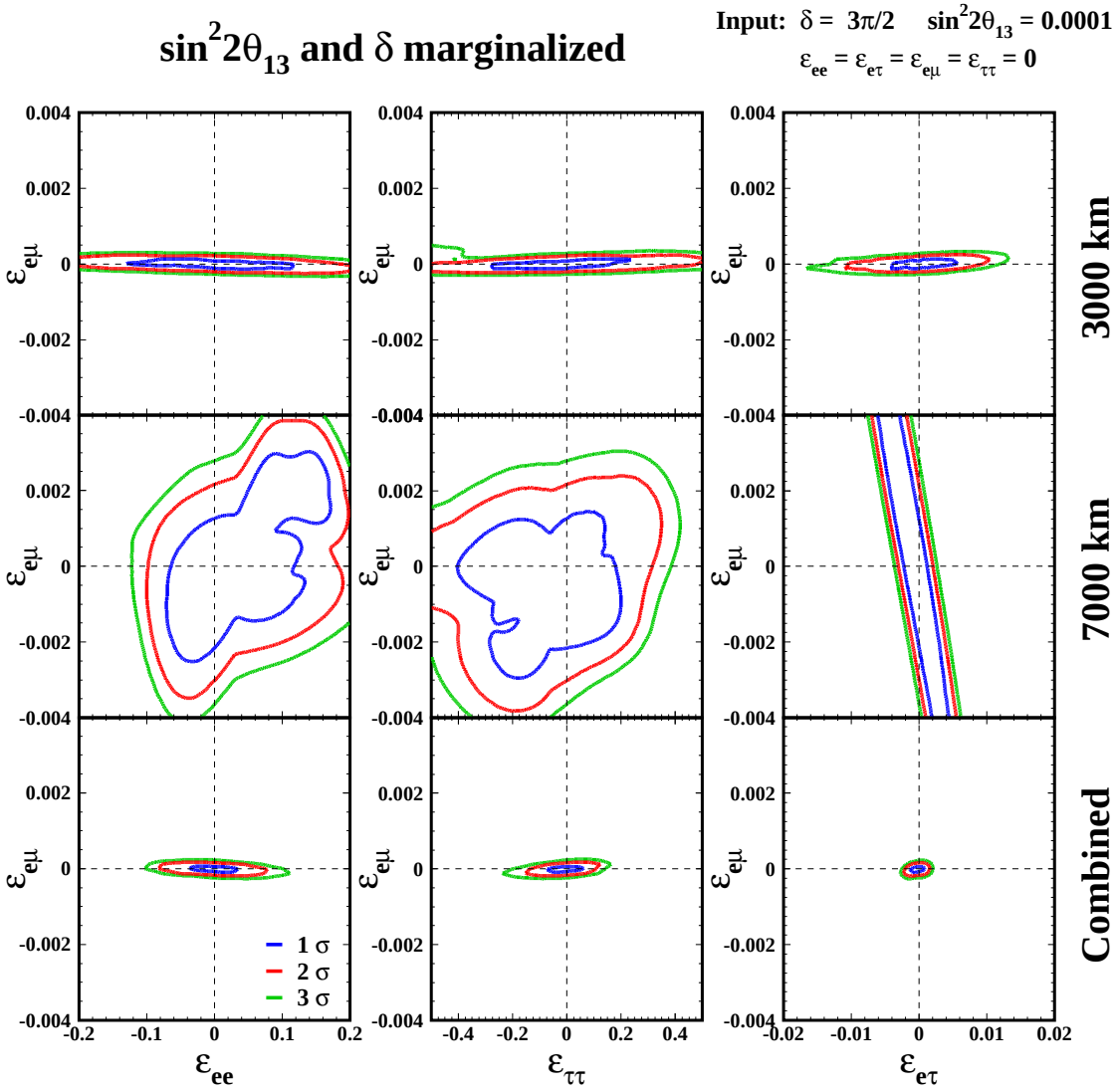

Figure 12: The same as in figure 6 but with $\sin^2 2\theta_{13} = 0.0001$.

mined by the two detector setting, and at the same time to what extent the measurement of θ_{13} and δ can be affected by non-zero input values of NSI. In this section, we examine the particular systems: $\varepsilon_{ee} - \varepsilon_{e\tau}$, $\varepsilon_{\tau\tau} - \varepsilon_{e\tau}$, and $\varepsilon_{ee} - \varepsilon_{\tau\tau}$. We do not discuss the case which involve $\varepsilon_{e\mu}$. The reason is that we want to take the NSI input values well below the current bounds presented eq. (2.2). The input value of $\varepsilon_{e\mu}$ which is comparable to the present constraint will not affect the sensitivity. In section 7, we will present more global informations. We work with the particular input values of θ_{13}, δ, and the ε parameters; $\sin^2 2\theta_{13} = 10^{-3}$, $\delta = 3\pi/2$, $\varepsilon_{e\tau} = 0.01$, $\varepsilon_{ee} = 0.1$, and $\varepsilon_{\tau\tau} = 0.2$. But, the features are not so different for other input values.

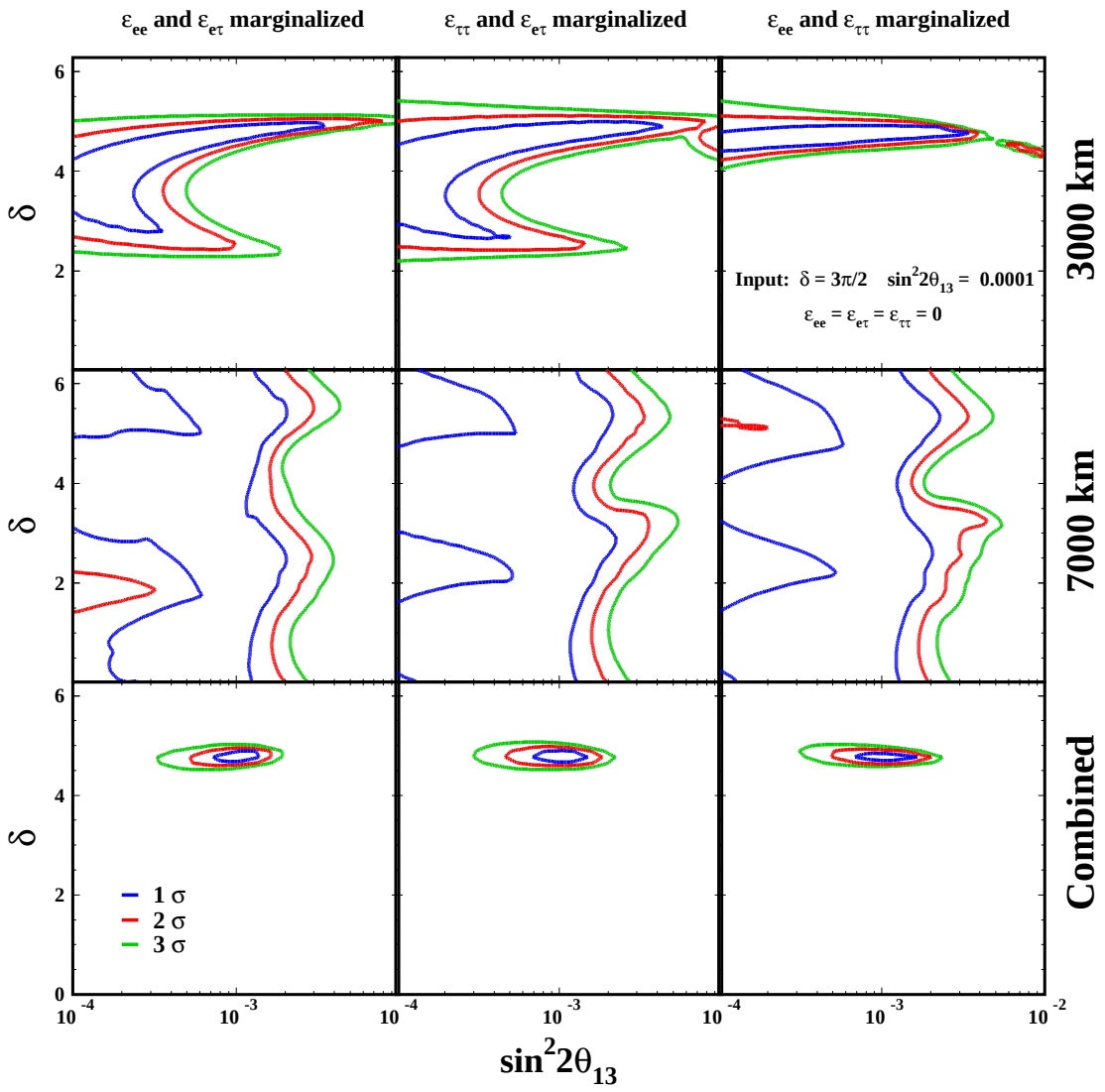

Figure 13: The same as in figure 9 but with $\sin^2 2\theta_{13} = 0.0001$.

6.1 Sensitivity to NSI, θ_{13}, and δ; case of non-zero input of NSI

Roughly speaking, the sensitivities to NSI, θ_{13}, and δ are not affected so much by the non-zero input values of ε's. This is because, even in the case of vanishing input, we freely vary them in fitting the data, and the presence of these extra degrees of freedom of varying over the NSI parameters is of key importance to determine (or affect) the sensitivities. Since the results are similar to the previous case, where NSI input were set to zero, we only present the figures for the case $\delta = 3\pi/2$. Generally speaking, the sensitivity is worse than for the case $\delta = \pi/4$. More or less one can guess what would be the general characteristics of this case from the figures with zero input, figures 3, 4, 7 and 8.

We first discuss the accuracy of the determination of NSI parameters. Presented in

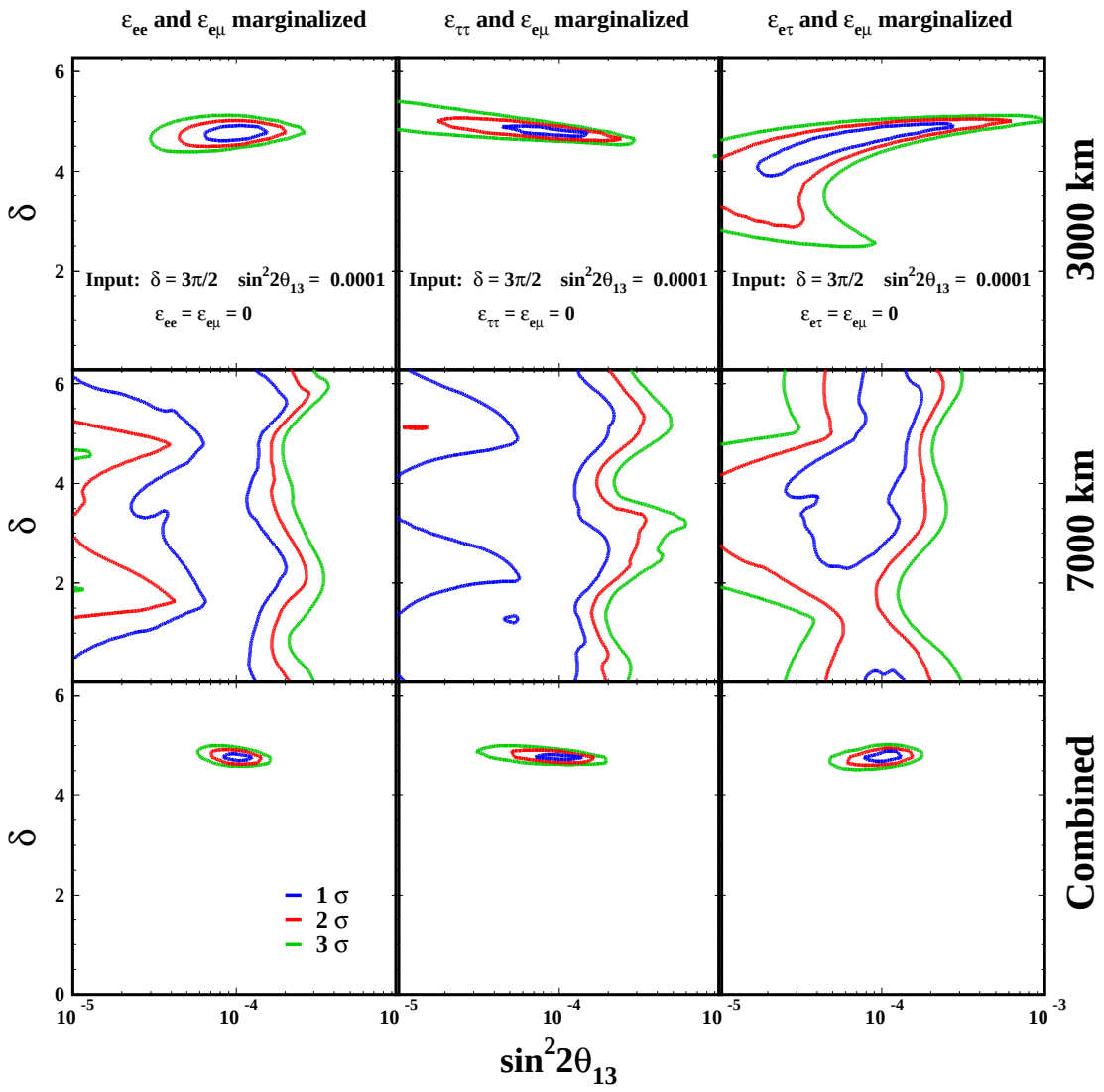

Figure 14: The same as in figure 10 but with $\sin^2 2\theta_{13} = 0.0001$.

figure 16 is the sensitivities to NSI parameters with the non-zero inputs. We notice that the features of the allowed regions are essentially the same as in the zero input case shown in figure 5. (About the two split islands in the middle panels see below.) We note that the accuracy of the determination of the ε parameters varies case by case. Most significantly, the size of allowed region of $\varepsilon_{e\tau}$, ε_{ee}, and $\varepsilon_{\tau\tau}$ become worse by more than a factor 2 in $\varepsilon_{ee} - \varepsilon_{e\tau}$ and $\varepsilon_{\tau\tau} - \varepsilon_{e\tau}$ systems. However, the accuracy of the determination of $\varepsilon_{e\tau}$ and $\varepsilon_{\tau\tau}$ at $\delta = \pi/4$ (not shown) improves by a factor of $\simeq 2$ with the non-zero input values of NSI.

Next, we discuss the accuracy of the measurement of θ_{13} and δ in the presence of non-vanishing input values of NSI. Figure 17 serves for this purpose. Again the features of figure 17 are similar to those of figure 9. We, however, notice some new characteristics. The

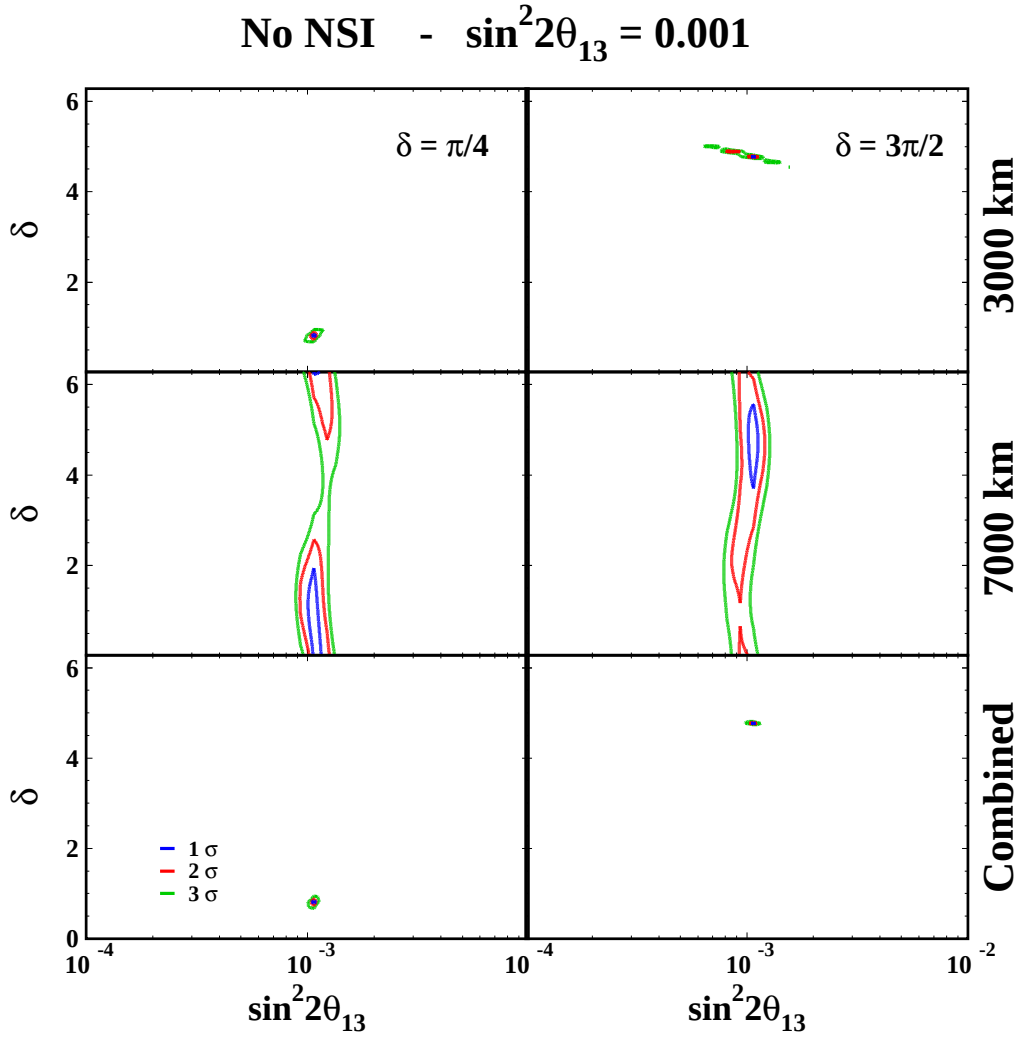

Figure 15: Allowed regions in the plane $\sin^2 2\theta_{13} - \delta$ for the standard oscillation case (no NSI) for the input values $\sin^2 2\theta_{13} = 0.001$, $\delta = \pi/4$ (left panels) and $\delta = 3\pi/2$ (right panels). The allowed regions were computed for 2 DOF. The experimental conditions are the same as for figure 7.

θ_{13}-NSI confusion at $L = 3000$ km is severer for $\delta = 3\pi/2$, but it is milder for $\delta = \pi/4$ (not shown) in the present case compared to zero ε input. Therefore, the degree of confusion depends very much on δ. Also the resultant accuracy of the determination of θ_{13} and δ, after the two detectors are combined, depends upon which ε is tuned on and also on δ though only mildly. For $\delta = 3\pi/2$, the uncertainty on $\sin^2 2\theta_{13}$ is smaller (larger) for the case of non-zero input value of the NSI parameters than for the zero-input case in the $\varepsilon_{\tau\tau} - \varepsilon_{e\tau}$ ($\varepsilon_{ee} - \varepsilon_{e\tau}$) system. It is interesting (and encouraging) to observe that non-zero input values of NSI essentially do not disturb the sensitivities to the determination of the NSI parameters but also the sensitivities to θ_{13} and δ.

JHEP12(2007)002

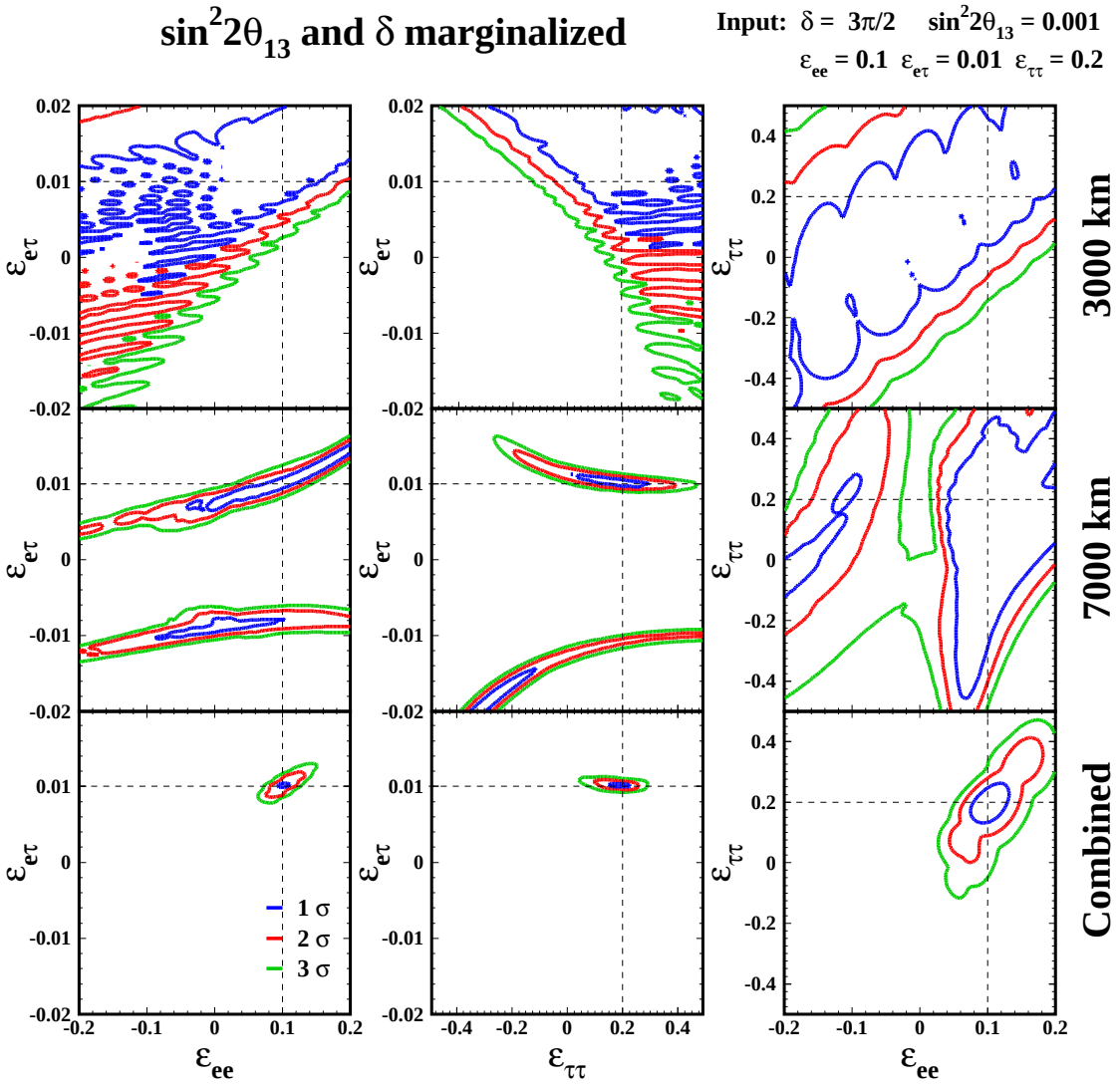

Figure 16: The same as in figure 5 but for non-vanishing input values of ε; $\varepsilon_{ee} = 0.1$, $\varepsilon_{e\tau} = 0.01$ and $\varepsilon_{\tau\tau} = 0.2$. We note that only the input values of 2 ε's are set to be non-zero at the same time. The thin dashed lines indicate the corresponding non-zero values of $\varepsilon_{\alpha\beta}$ for each panel.

6.2 Parameter degeneracies with and without NSI

In this subsection we want to make some remarks on the degeneracies associated with the measurement of NSI parameters as well as θ_{13} and δ. In figure 16, we observe two clearly separated islands in the regions allowed by the far detector measurement (middle panels) for the $\varepsilon_{\tau\tau} - \varepsilon_{e\tau}$ and the $\varepsilon_{ee} - \varepsilon_{e\tau}$ systems. A similar structure exists also in the combinations involving $\varepsilon_{e\mu}$. There exits a degeneracy of solutions of ε's. It is easy to understand the cause of the degeneracy; It is due to the invariance under sign change of $\varepsilon_{e\tau}$ that can be absorbed by rotation of δ by π. The fact that the symmetry exists only at the magic

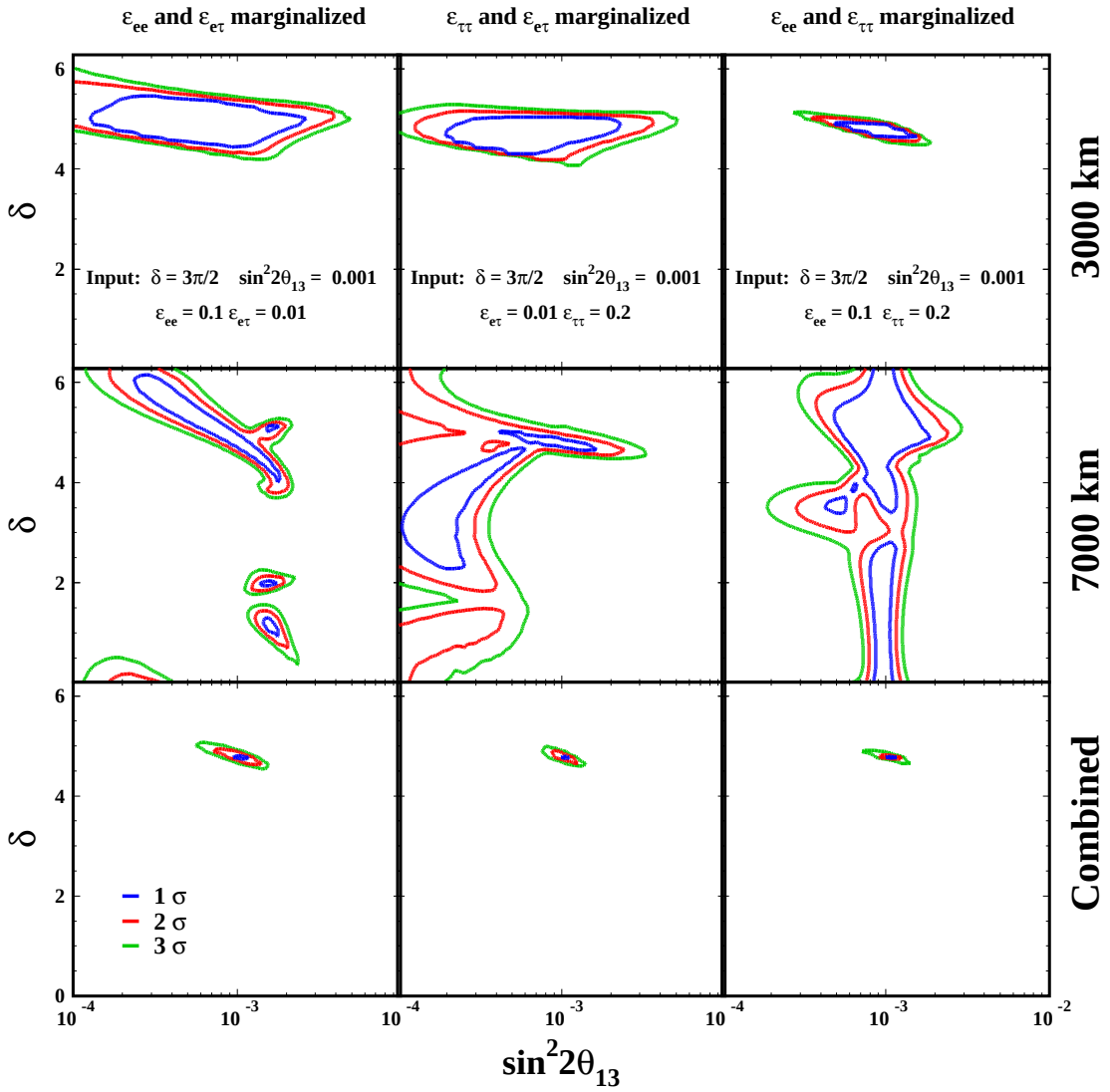

Figure 17: The same as in figure 9 but for non-vanishing input values of ε; $\varepsilon_{\rm ee} = 0.1$, $\varepsilon_{e\tau} = 0.01$ and $\varepsilon_{\tau\tau} = 0.2$.

baseline can be easily seen by comparing eqs. (A.25) and (3.2). This is also true in the corresponding formula with $\varepsilon_{e\mu}$ that one can derive from eq. (A.27). Since δ is marginalized the two clones appear in the allowed regions in the $\varepsilon_{\tau\tau} - \varepsilon_{e\tau}$ and $\varepsilon_{\rm ee} - \varepsilon_{e\tau}$ space.[6]

When the measurement at the two detectors, intermediate and far, are combined we obtain a unique allowed region; The degeneracy is resolved. It must be the case because there is no such symmetry in the whole system, see eq. (A.25) or (A.27). But, it is nice to see that it actually occurs in the concrete two detector setting adopted in this paper.

[6]If one wants to interpret this symmetry as the one which exist in the truncated system in which Δm^2_{21} is artificially switched off, it is a discrete version of the two phase degeneracy discussed in section 2.2.

We want to make brief remarks on the conventional parameter degeneracy [31, 33, 34] which would affect the sensitivity to the lepton mixing parameter. It might also affect the sensitivity to NSI through its effect to θ_{13} and δ. First of all, there is no θ_{23} octant degeneracy because θ_{23} is held fixed to $\pi/4$ in our analysis. With regard to the four-fold $\theta_{13} - \delta$ degeneracy duplicated by the unknown sign of Δm^2_{31} we have no hint for its existence in our analysis, apart from some limited cases at $\sin^2 2\theta_{13} = 10^{-4}$ which might be affected by it. The reason for this observation is that the clone solutions have a significantly different value of δ from the true solution (very roughly speaking $\delta_{\rm clone} \approx \pi - \delta_{\rm true}$), in both the intrinsic and the sign-Δm^2_{31} degeneracies. Nonetheless, from the figures we presented (and also in all those not shown) these is no such clone region. The reasons are: (1) The intrinsic degeneracy is resolved by the spectrum information[7], and (2) With long enough baselines the mass hierarchy is determined. Therefore, we suspect that the conventional parameter degeneracy plays minor role, if any, in our sensitivity analysis, except for the one associated with θ_{23} which we do not consider in this work.

7. Discovery reach to NSI, θ_{13} and δ

In this section we try to summarize the sensitivities to NSI, θ_{13} and δ that can be achieved by a neutrino factory with the intermediate-far detector setting. However, in looking for ways to present the sensitivities, we recognized that the sensitivities depend very much on the input values of δ and θ_{13}. Therefore, we need to show the sensitivities as a function of both δ and θ_{13} simultaneously.

In figures 18–22 we have presented the equi-uncertainty contours of a particular observable O in the plane spanned by the input values of $\sin^2 2\theta_{13}$ and δ. We have defined the uncertainty of measuring (or constraining) the observable O as $\Delta O \equiv (O_{\rm max} - O_{\rm min})/2$, except for the case of $\sin^2 2\theta_{13}$, where we give the fractional uncertainty, i.e. $\Delta(\sin^2 2\theta_{13})/\sin^2 2\theta_{13}$. For all cases we present the 2σ CL (2 DOF) contours.

The sensitivity to the NSI parameters, θ_{13} and δ can be determined in the analysis of the 6 combinations of NSI elements we have examined in this work: $\varepsilon_{ee} - \varepsilon_{e\mu}$, $\varepsilon_{ee} - \varepsilon_{e\tau}$, $\varepsilon_{ee} - \varepsilon_{\tau\tau}$, $\varepsilon_{e\mu} - \varepsilon_{e\tau}$, $\varepsilon_{e\mu} - \varepsilon_{\tau\tau}$ and $\varepsilon_{e\tau} - \varepsilon_{\tau\tau}$. Therefore we need altogether 12 panels to fully present the sensitivities to the ε's, and 12 panels present the sensitivities to the standard oscillation parameters θ_{13} (6 panels) and δ (6 panels).

We show, for definiteness, the case the NSI parameters have zero (vanishingly small) input values. But, as we saw in section 6, the results would not be so different even if we had taken non-zero input values for the NSI. Prior to showing the sensitivity contours we wish to warn the readers; Some of the structures are due to the finite grid used in our calculation, so the precise shape of the contours may not be reliable.

Let us first look at figures 18 and 19 where we show the sensitivity to the NSI parameters. Roughly speaking, for the typical value $\sin^2 2\theta_{13} \sim 10^{-3}$ the sensitivity to $\varepsilon_{\tau\tau}, \varepsilon_{ee}, \varepsilon_{e\tau}$ and $\varepsilon_{e\mu}$ are $\sim$ 10-20%, 2-10%, 0.1-0.4% and 0.01-0.04%, respectively. As we have discussed in previous sections, the off-diagonal NSI parameters have a much more significant impact

[7] We have confirmed that the intrinsic degeneracy survives the rate only analysis.

than that of the diagonal ones. We confirm here that in fact, they can be significantly more constrained by data. We observe that the sensitivity to the off-diagonal NSI parameters is basically not affected by the presence of another non-zero NSI contribution, whereas this is not true for the sensitivity to the diagonal elements. We suspect that this comportment may continue to be true even if more NSI parameters are switched on simultaneously.

Some of the features of these contours can be readily understood from the bi-probability plots in figure 1. For example, from panel (b2) of figure 18 and panels (d2) and (f1) of figure 19, we observe that the sensitivity to $\varepsilon_{e\tau}$ is best at $\delta = 0$ and $\delta = \pi$ and worst at $\delta = \pi/2$ and $3\pi/2$. This is exactly what one would expect from the upper right panel of figure 1, namely, the points in $P - \bar{P}$ space corresponding to $\delta = \pi/2$ (square) and $\delta = 3\pi/2$ (diamond) with non-zero $\varepsilon_{e\tau}$ can be confused with that of the standard case without NSI effect (orange strip). One can also understand that this behavior does not depend on θ_{13}.

Despite the contours for ε_{ee} have a more complicated structure, one can guess from the upper left panel of figure 1 that the best sensitivity should be for $\delta \sim 0 - \pi/4$ and worse for $\delta \sim \pi$. This is also confirmed by panels (a1), (b1) and (c1) of figure 18.

The sensitivity to $\varepsilon_{e\mu}$ shows an intricate dependence on δ and θ_{13} as seen in figure 18(a2) and figures 19(d1) and (e1). The sensitivity is the worst at around $\delta \simeq \pi/2$ and $\simeq 3\pi/2$ for $\sin^2 2\theta_{13} \sim 10^{-2}$, and at around $\delta \simeq \pi$ for $\sin^2 2\theta_{13} \sim 10^{-3}$. At $\sin^2 2\theta_{13} \sim 10^{-4}$, the sensitivity to $\varepsilon_{e\mu}$ has no significant dependence on δ. Let us understand the cause of such complicated features. First of all, the sensitivity to $\varepsilon_{e\mu}$ is coming dominantly from the measurement at 3000 km, as indicted in figures 4, 6 and 12. Then, it should be possible to understand the behavior at $\sin^2 2\theta_{13} \sim 10^{-3}$ from the bi-probability plot give in figure 2. This is indeed the case; The upper middle panel of the bi-probability plot shows that the ellipses of positive and negative $\varepsilon_{e\mu}$ as well as the one without NSI overlap with each other at $\delta \sim \pi$, and hence the sensitivity is worst at $\delta \sim \pi$. The similar bi-probability plot for $\sin^2 2\theta_{13} \sim 10^{-2}$ (not shown) indicates that a positive, negative, and zero $\varepsilon_{e\mu}$ ellipses meet at $\delta \sim \pi/2$ and $\sim 3\pi/2$. (Precise values of the crossing point are at around $\delta = 0.6\pi$ and 1.4π.) At $\sin^2 2\theta_{13} \sim 10^{-4}$ (not shown) there is no particular value of δ at which these ellipses overlap. Thus, these features of the bi-probability plots explain the behavior of sensitivity contours of $\varepsilon_{e\mu}$ in figure 18(a2) and figures 19(d1) and (e1).

Let us also discuss the sensitivity reach of θ_{13} and δ with and without NSI effect. In figure 20 we show the iso-contours of uncertainty on the determination of the CP phase δ (upper panel) and of $\sin^2 2\theta_{13}$ (lower panel) in the plane spanned by the input (true) values of $\sin^2 2\theta_{13}$ and δ in the absence of NSI effect. These results must be compared with the case with NSI effect we will show below.

In figure 21 we show the iso-uncertainty contour of the CP phase δ in the presence of NSI parameters for the 6 different combinations of the 2 ε systems we considered in this work. Roughly speaking, for the typical input value $\sin^2 2\theta_{13} \sim 10^{-3}$ the sensitive become worse when NSI is included. Nevertheless, the change is from $\Delta\delta \simeq 0.05 - 0.1$ radians (without NSI) to $\simeq 0.1 - 0.15$ radians or so (with NSI), in all 6 cases. We conclude that the difference between the sensitivities to δ with and without NSI is not dramatic.

On the other hand, regarding the sensitivity to $\sin^2 2\theta_{13}$, comparing the lower panel of figure 20 with figure 22, we can see that for the typical input value $\sin^2 2\theta_{13} \sim$

JHEP12(2007)002

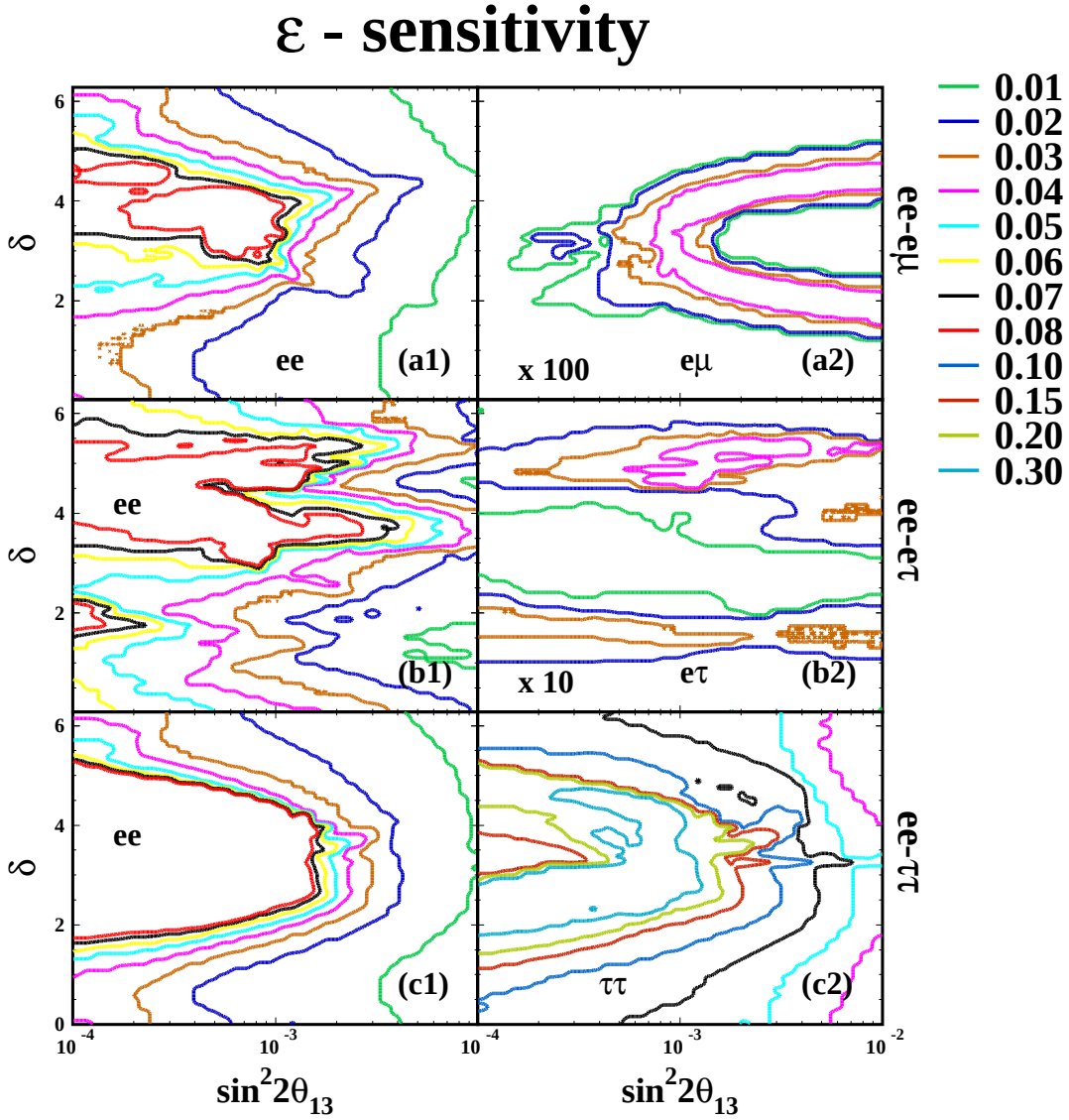

Figure 18: Iso-contours of 2 σ CL (for 2 DOF) sensitivity (uncertainty) for $\varepsilon_{\alpha\beta}$ parameter as functions of the input parameters of $\sin^2 2\theta_{13}$ and δ. For each point in the $\sin^2 2\theta_{13} - \delta$ plane the uncertainty is defined as $\Delta\varepsilon \equiv (\varepsilon_{\rm max} - \varepsilon_{\rm min})/2$ where $\varepsilon_{\rm max(min)}$ indicates the maximum and minimum allowed value of ε parameters which is consistent with the case without NSI effect. In the upper, lower and bottom panels, the sensitivities for (a1) $\varepsilon_{\rm ee}$ and (a2) $\varepsilon_{e\mu}$ for the $\varepsilon_{\rm ee}$-$\varepsilon_{e\mu}$ system, (b1) $\varepsilon_{\rm ee}$ and (b2) $\varepsilon_{e\tau}$ for the $\varepsilon_{\rm ee}$-$\varepsilon_{e\tau}$ system, and (c1) $\varepsilon_{\rm ee}$ and (c2) $\varepsilon_{\tau\tau}$ for the $\varepsilon_{\rm ee}$-$\varepsilon_{\tau\tau}$ system, respectively, are shown. We note that the the uncertainty for $\varepsilon_{e\mu}$ shown in (a2) and $\varepsilon_{e\tau}$ shown in (b2) are magnified by 100 and 10, respectively. Some of the structures are due to the finite grid used in our calculation, so the precise shape of the contours may not be reliable.

10^{-3} the fractional uncertainty on $\sin^2 2\theta_{13}$ becomes larger with NSI, going from $\Delta(\sin^2 2\theta_{13})/\sin^2 2\theta_{13} \sim 10\%$ (without NSI) to $\sim 10 - 20\%$ (with NSI). Again we conclude that the impact of NSI in the determination of θ_{13} is not so striking.

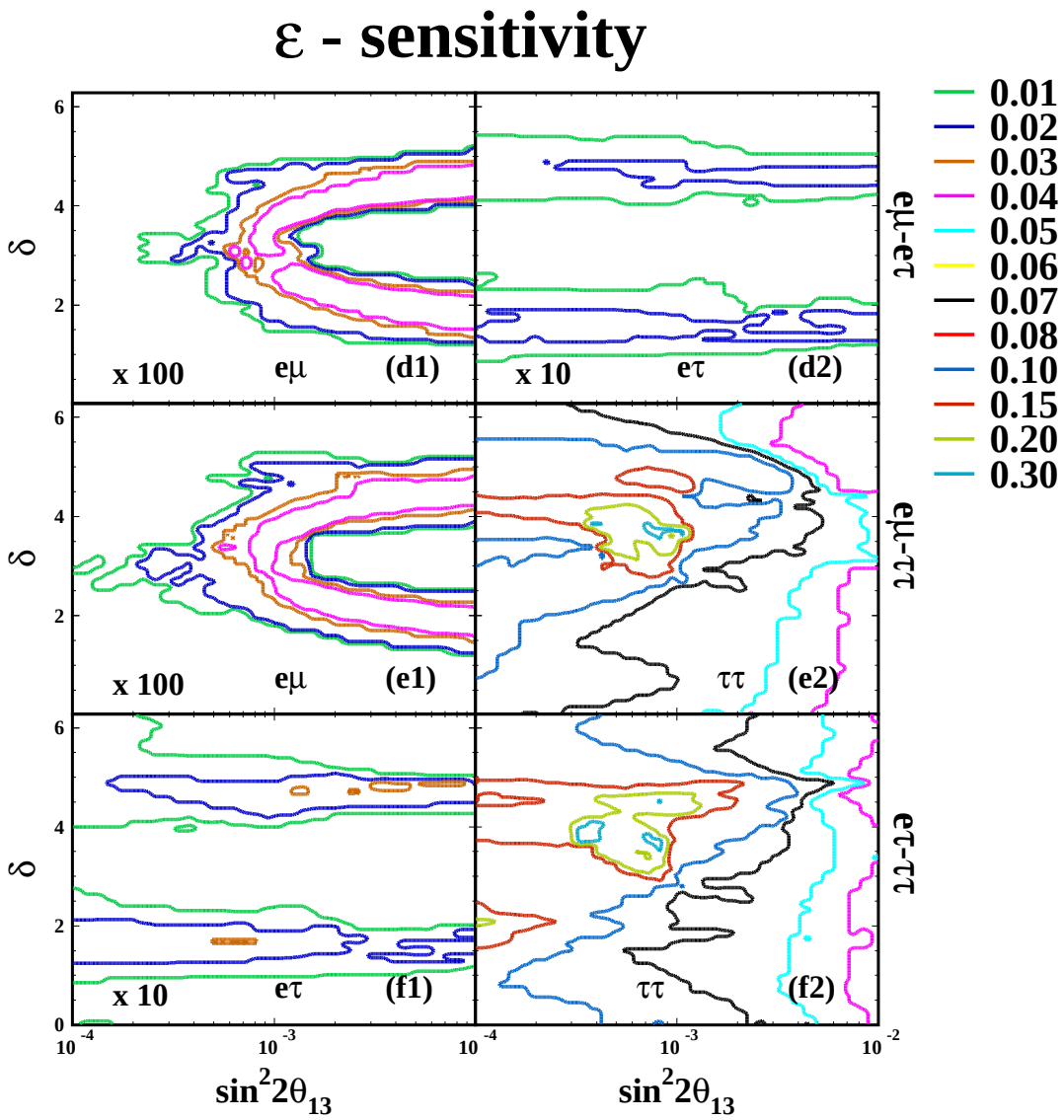

Figure 19: Same as in figure 18 but for different combination of the 2 ε system. In the upper, lower and bottom panels, the sensitivities for (d1) $\varepsilon_{e\mu}$ and (d2) $\varepsilon_{e\tau}$ for the $\varepsilon_{e\mu}$-$\varepsilon_{e\tau}$ system, (e1) $\varepsilon_{e\mu}$ and (e2) $\varepsilon_{\tau\tau}$ for the $\varepsilon_{e\mu}$-$\varepsilon_{\tau\tau}$ system, and (f1) $\varepsilon_{e\tau}$ and (f2) $\varepsilon_{\tau\tau}$ for the $\varepsilon_{e\tau}$-$\varepsilon_{\tau\tau}$ system, respectively, are shown. As in figure 18 the uncertainty for $\varepsilon_{e\mu}$ shown in (d1) and (e1) and $\varepsilon_{e\tau}$ shown in (d2) and (f1) are magnified by 100 and 10, respectively.

8. Concluding remarks

We have demonstrated in this paper that a neutrino factory equipped with an intense neutrino flux from a muon storage ring and two detectors, one located at $L = 3000$ km and the other at $L = 7000$ km, is powerful enough to probe into extremely small values of the NSI parameters. We have relied on the golden channel, $\nu_e \to \nu_\mu$, and its anti-neutrino counter part in our analysis in this paper. Six different combinations of the two ε systems

that can be obtained from the four NSI parameters, $\varepsilon_{\alpha\beta}$ with (α, β) being (e, e), (τ, τ), (e, μ) and (e, τ), are analyzed under the assumption of ignoring the effects of NSI at the production and the detection of neutrinos.

The sensitivities to off-diagonal ε's are excellent, $|\varepsilon_{e\tau}| \simeq$ a few $\times 10^{-3}$ and $|\varepsilon_{e\mu}| \simeq$ a few $\times 10^{-4}$ and while the ones for the diagonal ε's are acceptable, $|\varepsilon_{ee}|(|\varepsilon_{\tau\tau}|) \simeq 0.1(0.2)$ at 3σ CL and 2 DOF. These sensitivities remain more or less independent of θ_{13} down to extremely small values such as $\sin^2 2\theta_{13} = 10^{-4}$. They seem also very robust in the sense that they are not very disturbed by the presence of another non-zero NSI contribution. The above characteristics of the sensitivities to NSI suggest that in our setting the off-diagonal ε's are likely the best place to discover NSI. We note that these results are obtained under the assumption of ignoring background as well as systematic errors in our analysis. According to our estimate, however, the effect of inclusion of them is limited to $\sim 50\%$ (a factor of 2) or so for θ_{13} as small as $\sin^2 2\theta_{13} = 10^{-3}$ (10^{-4}).

One of the most significant features of the results obtained in our analysis is that the presence of NSI *does not* confuses the precision measurement of θ_{13} and δ. The favorite property arises from the synergy between the two detectors placed at the two different baselines; The detector at the magic baseline is extremely (reasonably) sensitive to the off-diagonal (diagonal) ε's but lack sensitivity to δ. On the other hand, the intermediate detector at $L = 3000$ km *is* sensitive to δ, while lacking good sensitivity to ε's (except in the case of $\varepsilon_{e\mu}$). We have shown in section 5 and 6 that, when combined, the synergy between the two detectors has an enormous power to resolve the confusion between θ_{13} and NSI. Moreover, the impact of the systematic errors on δ and θ_{13} is limited especially at small θ_{13} and at most $\sim$10%-20% level at $\sin^2 2\theta_{13} = 10^{-4}$. We believe that the results obtained in this paper open the door to the possibility of using neutrino factory as a discovery machine for NSI.

Our analysis in this paper, however, has limitations of validity because we have assumed that the effects of NSI in production and the detection processes are negligible. It may be a self-consistent approximation when we discuss the $\varepsilon_{e\tau}$ system, assuming a very small $\varepsilon_{e\tau}$, because its effect on muon decay is expected to be small. But, if we discuss the $\varepsilon_{e\mu}$ system it affects the production and the detection processes at one-loop level and all these effects have to be consistently dealt with. In this paper we are not able to address this point. Our analysis also does not include the energy resolution and the uncertainty on the matter density as well as on the remaining mixing parameters.

We have also mentioned in section 2 that the phase of the off-diagonal $\varepsilon_{\alpha\beta}$ produces confusion problems of two types, the two-phase and the phase-magnitude confusion. In our analysis we have shown that the discrete version of the former degeneracy is resolved by the two-detector setting examined in this paper. Therefore, it is natural to expect that the degeneracies in its generic form as well as the latter type will also be resolved by the two-detector setting. The magnitudes of the solar Δm^2_{21} sensitive terms will be different between the intermediate and the far detectors so that the confusions will be lifted by combining them. The work toward this direction is in progress.

One could think about adding the silver channel in the analysis [48]. This could, in principle, increase the sensitivity to $\epsilon_{\tau x}$. In the present setting of magnetized iron detectors it

requires separation of muons produced by tau decay from those of oscillated ν_μ CC reaction. This requires more sophisticated analysis and therefore it is left for future investigation.

Acknowledgments

Four of us (H.M., H.N., S.U. and R.Z.F) are grateful for the hospitality of the Theory Group of the Fermi National Accelerator Laboratory during the summer of 2007 where this work was completed. H.M. and R.Z.F thank Departamento de Física, Pontifícia Universidade Católica do Rio de Janeiro, where part of this work was carried out, for the hospitality. This work was supported in part by KAKENHI, Grant-in-Aid for Scientific Research, No 19340062, Japan Society for the Promotion of Science, by Fundação de Amparo à Pesquisa do Estado de São Paulo (FAPESP), Fundação de Amparo à Pesquisa do Estado de Rio de Janeiro (FAPERJ) and Conselho Nacional de Ciência e Tecnologia (CNPq).

A. Derivation of appearance probability $P(\nu_e \to \nu_\mu)$ in the presence of non-standard interactions

In this appendix, we give a self-contained discussion for deriving the expression of appearance probability $P(\nu_e \to \nu_\mu)$ with simultaneous presence of non-standard interactions ε_{ee} and $\varepsilon_{e\tau}$. For simplicity, we denote it $\varepsilon_{e\tau} - \varepsilon_{ee}$ system, and use the method developed by Kimura, Takamura, and Yokomakura (KTY) [49]. (See [50] for minor sign error in the original formula, and [40] for a reformulation.)

The evolution equation of neutrinos can be written in the flavor eigenstate as

$$i\frac{d}{dx}\nu_\alpha = \frac{1}{2E}H_{\alpha\beta}\nu_\beta \qquad (\alpha, \beta = e, \mu, \tau), \tag{A.1}$$

where the Hamiltonian is given by

$$H = U\begin{bmatrix} \Delta m^2_{11} & 0 & 0 \\ 0 & \Delta m^2_{21} & 0 \\ 0 & 0 & \Delta m^2_{31} \end{bmatrix} U^\dagger + a(x)\begin{bmatrix} 1+\varepsilon_{ee} & 0 & \varepsilon_{e\tau} \\ 0 & 0 & 0 \\ \varepsilon^*_{e\tau} & 0 & 0 \end{bmatrix}, \tag{A.2}$$

whose first term will be denoted as $H^{\rm vac}$ hereafter and $\Delta m^2_{ji} \equiv m^2_j - m^2_i$. (Hence, $\Delta m^2_{11} \equiv 0$ by definition.) In (A.2), $a \equiv 2\sqrt{2}G_F n_e(x)E$ denotes the coefficient related to the index of refraction of neutrinos in medium [3] with electron number density $n_e(x)$, where G_F is the Fermi constant and E is the neutrino energy. Despite that $n_e(x)$ may depend upon locations along the neutrino trajectory, we use constant density approximation throughout this paper. The MNS matrix U relates the flavor and the vacuum mass eigenstates as

$$\nu_\alpha = (U)_{\alpha i}\nu_i, \tag{A.3}$$

where i runs over 1-3. We use the standard parametrization of the MNS matrix [51];

$$U = \begin{bmatrix} c_{12}c_{13} & s_{12}c_{13} & s_{13}e^{-i\delta} \\ -s_{12}c_{23} - c_{12}s_{23}s_{13}e^{i\delta} & c_{12}c_{23} - s_{12}s_{23}s_{13}e^{i\delta} & s_{23}c_{13} \\ s_{12}s_{23} - c_{12}c_{23}s_{13}e^{i\delta} & -c_{12}s_{23} - s_{12}c_{23}s_{13}e^{i\delta} & c_{23}c_{13} \end{bmatrix}, \tag{A.4}$$

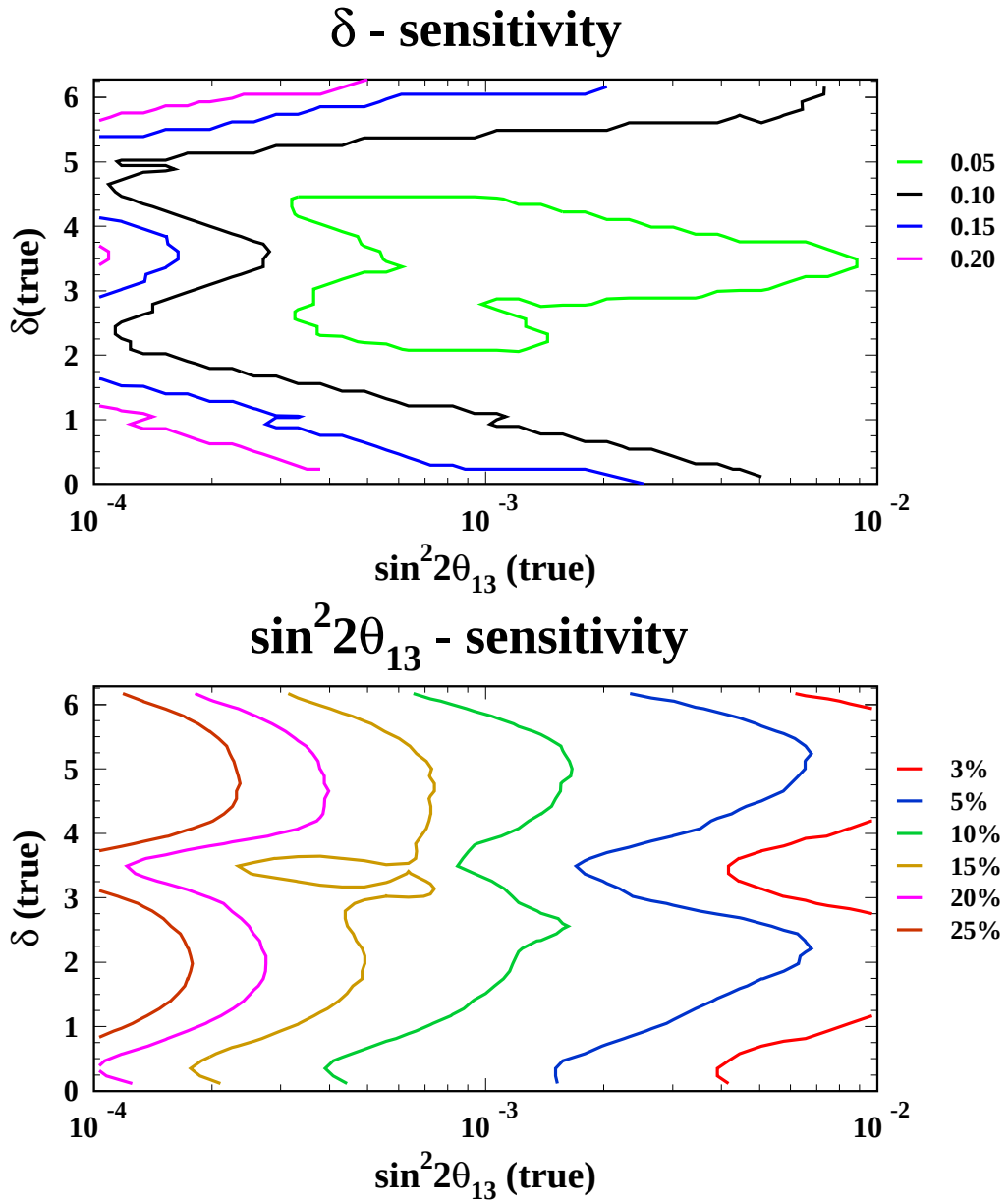

Figure 20: Upper panel: Iso-contours of 2 σ CL (for 2 DOF) sensitivity (uncertainty) for the CP phase δ (in radians) expected to be achieved at neutrino factory in the absence of the NSI effect in the plane of the true values of δ and $\sin^2 2\theta_{13}$. The uncertainty is defined as $\Delta\delta \equiv (\delta_{\rm max} - \delta_{\rm min})/2$ in radians, where $\delta_{\rm max(min)}$ is maximum (minimum) allowed value of δ (mod. 2π) for each given input point. Lower panel: Similar plot as in the upper panel but for the fractional uncertainty $\Delta(\sin^2 2\theta_{13})/\sin^2 2\theta_{13}$ (in percent) is shown.

where c_{ij} and s_{ij} $(i, j = 1\text{-}3)$ imply $\cos\theta_{ij}$ and $\sin\theta_{ij}$, respectively.

By defining renormalized matter coefficient and renormalized $\varepsilon_{e\tau}$ as

$$\tilde{a} \equiv a(1 + \varepsilon_{ee}) \qquad\qquad \tilde{\varepsilon}_{e\tau} \equiv \frac{\varepsilon_{e\tau}}{1 + \varepsilon_{ee}} \tag{A.5}$$

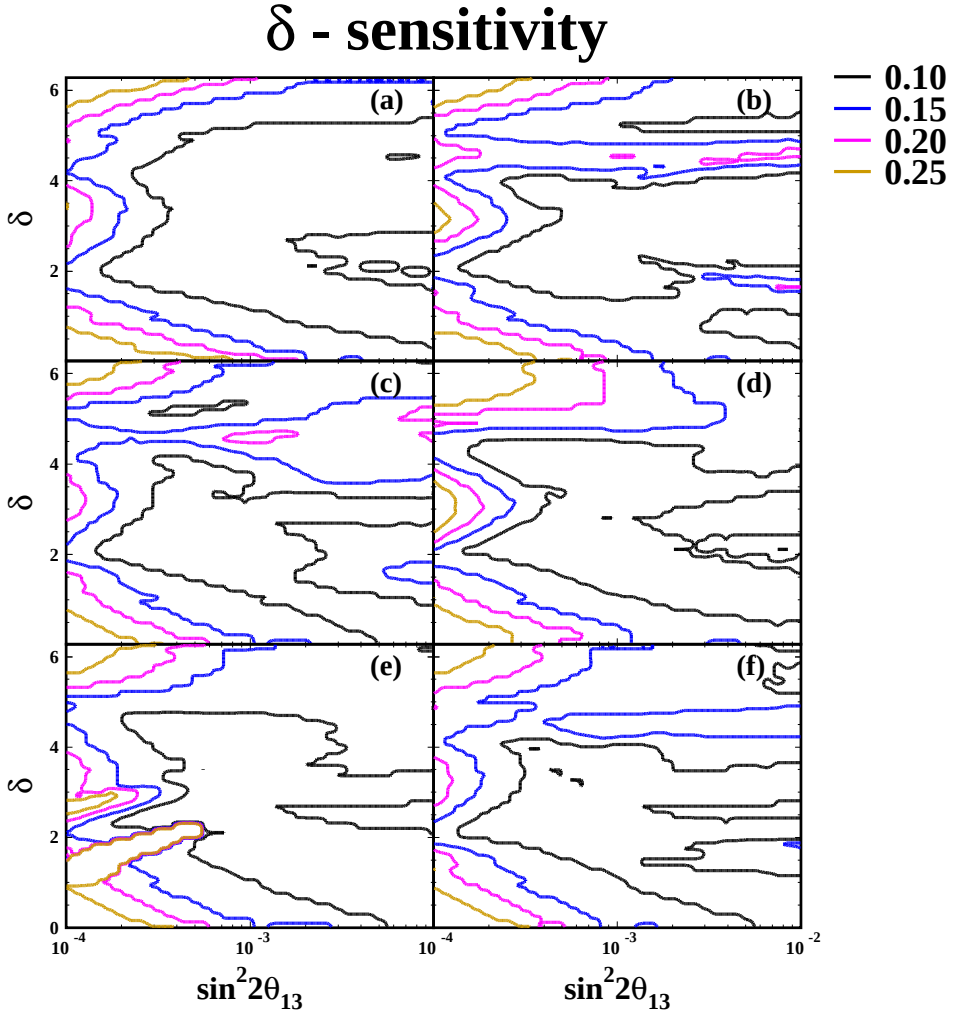

Figure 21: Same as in the upper panel of figure 20 but for the case where the NSI parameters are turned on in the fit. The iso-contours of $\Delta\delta$ (in radians) at 2 σ CL (for 2 DOF) are shown for the 6 combinations of 2 ε system: (a) $\varepsilon_{ee} - \varepsilon_{e\mu}$, (b) $\varepsilon_{ee} - \varepsilon_{e\tau}$, (c) $\varepsilon_{ee} - \varepsilon_{\tau\tau}$, (d) $\varepsilon_{e\mu} - \varepsilon_{e\tau}$, (e) $\varepsilon_{e\mu} - \varepsilon_{\tau\tau}$ and (f) $\varepsilon_{e\tau} - \varepsilon_{\tau\tau}$.

the matter term in the Hamiltonian can be written as

$$\tilde{a} \begin{bmatrix} 1 & 0 & \tilde{\varepsilon}_{e\tau} \\ 0 & 0 & 0 \\ \tilde{\varepsilon}^*_{e\tau} & 0 & 0 \end{bmatrix}. \tag{A.6}$$

Thus, the problem is reduced to the effective system with only single type of NSI, $\tilde{\varepsilon}_{e\tau}$.

We now define the mass eigenstate in matter ν_i^m by using the transformation

$$\nu_\alpha = (V)_{\alpha i}\, \nu_i^m, \tag{A.7}$$

where V is the unitary matrix which diagonalize the Hamiltonian with scaled eigenvalues λ as $V^\dagger H V = H_{\rm diag} \equiv diag(a\lambda_1, a\lambda_2, a\lambda_3)$. We first obtain the expressions of the eigenvalues

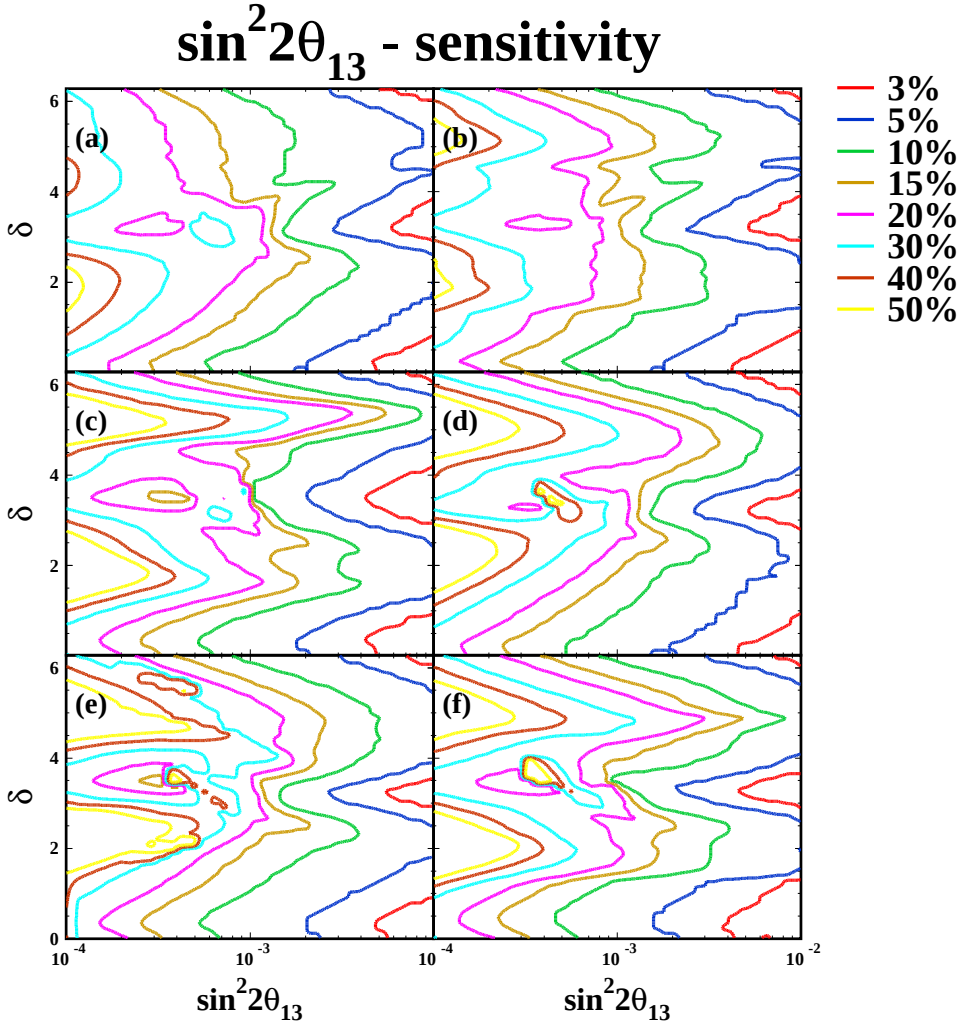

Figure 22: Same as in the lower panel of figure 20 but for the case where the NSI parameters are turned on in the fit. The iso-contours of $\Delta(\sin^2 2\theta_{13})/\sin^2 2\theta_{13}$ at 2 σ CL (for 2 DOF) are shown for the 6 combinations of 2 ε system: (a) $\varepsilon_{ee} - \varepsilon_{e\mu}$, (b) $\varepsilon_{ee} - \varepsilon_{e\tau}$, (c) $\varepsilon_{ee} - \varepsilon_{\tau\tau}$, (d) $\varepsilon_{e\mu} - \varepsilon_{e\tau}$, (e) $\varepsilon_{e\mu} - \varepsilon_{\tau\tau}$ and (f) $\varepsilon_{e\tau} - \varepsilon_{\tau\tau}$.

of the Hamiltonian (A.2). They are determined by the equation $det[H - \lambda aI] = 0$ which is the cubic equation for the scaled eigenvalue λ:

$$\begin{aligned}
&\lambda^3 - (1 + \delta_{31} + \delta_{21})\lambda^2 \qquad\qquad (A.8)\\
&+\Big[c_{13}^2\delta_{31} + \left\{\delta_{31} + c_{12}^2 + s_{12}^2 s_{13}^2 + 2c_{12}s_{12}s_{23}c_{13}Re(\tilde{\varepsilon}_{e\tau})\right\}\delta_{21}\\
&\qquad\qquad -2c_{23}c_{13}s_{13}(\delta_{31} - s_{12}^2\delta_{21})Re(\tilde{\varepsilon}_{e\tau}e^{i\delta}) - |\tilde{\varepsilon}_{e\tau}|^2\Big]\lambda\\
&-\delta_{21}\delta_{31}\Big[c_{12}^2c_{13}^2 + 2c_{12}s_{12}s_{23}c_{13}Re(\tilde{\varepsilon}_{e\tau}) - 2c_{12}^2c_{23}c_{13}s_{13}Re(\tilde{\varepsilon}_{e\tau}e^{i\delta})\Big]\\
&\qquad +|\tilde{\varepsilon}_{e\tau}|^2\Big[s_{23}^2c_{13}^2\delta_{31} + (c_{12}^2c_{23}^2 + s_{12}^2s_{23}^2s_{13}^2 - 2c_{12}s_{12}c_{23}s_{23}s_{13}\cos\delta)\delta_{21}\Big] = 0.
\end{aligned}$$

in which everything is scaled by a and δ_{21} and δ_{31} denote the scaled squared mass

differences,

$$\delta_{21} \equiv \frac{\Delta m^2_{21}}{\tilde{a}}, \qquad \delta_{31} \equiv \frac{\Delta m^2_{31}}{\tilde{a}}. \tag{A.9}$$

A.1 KTY method for obtaining exact oscillation probability with NSI

We follow the KTY method [49] for deriving $P(\nu_e \to \nu_\mu)$ and write down the equations

$$\begin{aligned} H_{e\mu} &= H^{\rm vac}_{e\mu}, \\ H_{e\tau}H_{\tau\mu} - H_{e\mu}H_{\tau\tau} &= (H^{\rm vac}_{e\tau} + \tilde{\varepsilon}_{e\tau})H^{\rm vac}_{\tau\mu} - H^{\rm vac}_{e\mu}H^{\rm vac}_{\tau\tau}. \end{aligned} \tag{A.10}$$

They give relationships between mixing matrix in vacuum and in matter as

$$\begin{aligned} \sum_i \lambda_i V_{ei}V^*_{\mu i} &= \sum_i \delta_{j1}U_{ei}U^*_{\mu i} \equiv p, \\ \sum_{ijk}^{\rm cyclic} \lambda_j\lambda_k V_{ei}V^*_{\mu i} &= \sum_{ijk}^{\rm cyclic} \delta_{j1}\delta_{k1}U_{ei}U^*_{\mu i} + \tilde{\varepsilon}_{e\tau}\sum_i \delta_{i1}U_{\tau i}U^*_{\mu i} \equiv q. \end{aligned} \tag{A.11}$$

Notice that the effect of $\tilde{\varepsilon}_{e\tau}$ is contained only in q. Solving (A.11) for $V_{ei}V^*_{\mu i}$ under the constraint of unitarity $\sum_i V_{ei}V^*_{\mu i} = 0$ we obtain

$$V_{ei}V^*_{\mu i} = \frac{p\lambda_i + q}{\Delta_{ji}\Delta_{ki}} \tag{A.12}$$

where $\Delta_{ji} \equiv \lambda_j - \lambda_i$ and (i, j, k) are cyclic.

Then, the appearance probability $P(\nu_e \to \nu_e)$ is given exactly by [49],

$$\begin{aligned} P(\nu_e \to \nu_\mu) = 4\sum_{(ijk)}^{\rm cyclic} (&{\rm Re}\tilde{J}^{ij}_{e\mu} + {\rm Re}\tilde{J}^{jk}_{e\mu}) \cos\left(\frac{\tilde{a}L}{4E}\Delta_{ki}\right) \sin\left(\frac{\tilde{a}L}{4E}\Delta_{ij}\right) \sin\left(\frac{\tilde{a}L}{4E}\Delta_{jk}\right), \\ +8\sum_{(ijk)}^{\rm cyclic} &\tilde{J} \sin\left(\frac{\tilde{a}L}{4E}\Delta_{12}\right) \sin\left(\frac{\tilde{a}L}{4E}\Delta_{23}\right) \sin\left(\frac{\tilde{a}L}{4E}\Delta_{31}\right), \end{aligned} \tag{A.13}$$

where the sum over the cyclic permutation is implied and

$${\rm Re}\tilde{J}^{ij}_{e\mu} = \frac{|p|^2\lambda_i\lambda_j + |q|^2 + {\rm Re}(pq^*)(\lambda_i + \lambda_j)}{\Delta_{ij}\Delta_{12}\Delta_{23}\Delta_{31}}, \tag{A.14}$$

$$\tilde{J} = \frac{{\rm Im}(pq^*)}{\Delta_{12}\Delta_{23}\Delta_{31}}. \tag{A.15}$$

It is thus convenient to compute the combination ${\rm Re}\tilde{J}^{ij}_{e\mu} + {\rm Re}\tilde{J}^{jk}_{e\mu}$ (note the minus sign),

$${\rm Re}\tilde{J}^{ij}_{e\mu} + {\rm Re}\tilde{J}^{jk}_{e\mu} \equiv \frac{-1}{(\Delta_{ij}\Delta_{jk})^2} J_j \tag{A.16}$$

where

$$
\begin{aligned}
J_j &\equiv |p|^2\lambda_j^2 + 2\mathrm{Re}(pq^*)\lambda_j + |q|^2 \\
&= C_j + 2A_j^{(I)}\cos\delta + 2A_j^{(II)}\cos 2\delta + 2B_j^{(I)}\sin\delta + 2B_j^{(II)}\sin 2\delta \qquad \text{(A.17)} \\
C_j &= (p_0^2+p_1^2)\lambda_j^2 + 2\{p_0\mathrm{Re}(q_0)+p_1\mathrm{Re}(q_1)\}\lambda_j + |q_0|^2 + |q_1|^2 + |q_2|^2 \\
A_j^{(I)} &= p_0p_1\lambda_j^2 + \{p_0\mathrm{Re}(q_1+q_2)+p_1\mathrm{Re}(q_0)\}\lambda_j + \mathrm{Re}(q_0)\mathrm{Re}(q_1+q_2) + \mathrm{Im}(q_0)\mathrm{Im}(q_1+q_2) \\
A_j^{(II)} &= p_1\mathrm{Re}(q_2)\lambda_j + \mathrm{Re}(q_1)\mathrm{Re}(q_2) + \mathrm{Im}(q_1)\mathrm{Im}(q_2) \\
B_j^{(I)} &= \{p_0\mathrm{Im}(q_1-q_2) - p_1\mathrm{Im}(q_0)\}\lambda_j + \mathrm{Re}(q_0)\mathrm{Im}(q_1-q_2) - \mathrm{Im}(q_0)\mathrm{Re}(q_1-q_2) \\
B_j^{(II)} &= -p_1\mathrm{Im}(q_2)\lambda_j + \mathrm{Im}(q_1)\mathrm{Re}(q_2) - \mathrm{Re}(q_1)\mathrm{Im}(q_2) \qquad \text{(A.18)}
\end{aligned}
$$

$\tilde{J}$ is given by

$$
\tilde{J} = \frac{1}{\Delta_{12}\Delta_{23}\Delta_{31}}\Big[J^{(I)}\sin\delta + J^{(II)}\sin 2\delta + K^{(0)} + K^{(I)}\cos\delta + K^{(II)}\cos 2\delta\Big] \qquad \text{(A.19)}
$$

where

$$
\begin{aligned}
J^{(I)} &= \{p_0\mathrm{Re}(q_1-q_2) - p_1\mathrm{Re}(q_0)\} \\
J^{(II)} &= -p_1\mathrm{Re}(q_2) \\
K^{(0)} &= -p_0\mathrm{Im}q_0 - p_1\mathrm{Im}q_1 \\
K^{(I)} &= -\{p_0\mathrm{Im}(q_1+q_2) + p_1\mathrm{Im}(q_0)\} \\
K^{(II)} &= -p_1\mathrm{Im}(q_2) \qquad \text{(A.20)}
\end{aligned}
$$

The coefficients p and q, which are defined in (A.11), can be written as

$$
\begin{aligned}
p &= p_0 + p_1 e^{-i\delta} \\
q &= q_0 + q_1 e^{-i\delta} + q_2 e^{+i\delta} \qquad \text{(A.21)}
\end{aligned}
$$

where

$$
\begin{aligned}
p_0 &= \delta_{21}c_{12}s_{12}c_{23}c_{13}, \\
p_1 &= (\delta_{31} - s_{12}^2\delta_{21})s_{23}c_{13}s_{13} \\
q_0 &= -\delta_{31}\delta_{21}c_{12}s_{12}c_{23}c_{13} + \tilde{\varepsilon}_{e\tau}c_{23}s_{23}\Big[\delta_{31}c_{13}^2 - \delta_{21}(c_{12}^2 - s_{12}^2s_{13}^2)\Big]. \\
q_1 &= \delta_{21}\Big[-\delta_{31}c_{12}^2s_{23}c_{13}s_{13} + \tilde{\varepsilon}_{e\tau}c_{12}s_{12}s_{23}^2s_{13}\Big], \\
q_2 &= -\tilde{\varepsilon}_{e\tau}\delta_{21}c_{12}s_{12}c_{23}^2s_{13}. \qquad \text{(A.22)}
\end{aligned}
$$

Notice that the coefficient p is identical with the standard case without NSI interactions whereas q has a little more complex δ dependence with q_2 term and the coefficients q_i $(i = 1-3)$ have imaginary parts.

Collecting formulae given in the equations from (A.13) to (A.22) and using the exact eigenvalues by solving the cubic equation (A.8), we obtain the exact expression of the

appearance probability $P(\nu_e \to \nu_\mu)$ with the neutrino NSI ε_{ee} and $\varepsilon_{e\tau}$. Notice that $\tilde{a}$ and $\tilde{\varepsilon}_{e\tau}$ are the renormalized quantities defined by (A.5).

$$
\begin{aligned}
&P(\nu_e \to \nu_\mu; \varepsilon_{ee}, \varepsilon_{e\tau}) \\
&\quad = 8 \sum_{(ijk)}^{\text{cyclic}} \frac{-1}{(\Delta_{ij}\Delta_{jk})^2} \Big[\frac{1}{2} C_j + A_j^{(I)} \cos\delta + A_j^{(II)} \cos 2\delta + B_j^{(I)} \sin\delta + B_j^{(II)} \sin 2\delta \Big] \\
&\qquad \times \cos\left(\frac{\tilde{a}L}{4E}\Delta_{ki}\right) \sin\left(\frac{\tilde{a}L}{4E}\Delta_{ij}\right) \sin\left(\frac{\tilde{a}L}{4E}\Delta_{jk}\right), \\
&\qquad + 8 \frac{1}{\Delta_{12}\Delta_{23}\Delta_{31}} \Big[J^{(I)} \sin\delta + J^{(II)} \sin 2\delta + K^{(0)} + K^{(I)} \cos\delta + K^{(II)} \cos 2\delta \Big] \\
&\qquad \times \sin\left(\frac{\tilde{a}L}{4E}\Delta_{12}\right) \sin\left(\frac{\tilde{a}L}{4E}\Delta_{23}\right) \sin\left(\frac{\tilde{a}L}{4E}\Delta_{31}\right).
\end{aligned}
\tag{A.23}
$$

A.2 Leading order formula of $P(\nu_e \to \nu_\mu)$

Now, we define the perturbative scheme we use in our derivation of the approximate expression of the appearance probability $P(\nu_e \to \nu_\mu)$. We regard δ_{31} and a as of order unity, and assume that $s_{13} \simeq \delta_{21} \simeq \tilde{\varepsilon}_{e\tau}$ are small and are of the same order to organize the perturbation theory. We denote the expansion parameters symbolically as ϵ. We assume that $\epsilon \sim 10^{-2}$. If we organize the perturbation expansion in terms of ϵ we will recognize that the leading order terms in the oscillation probability in $P(\nu_e \to \nu_\mu)$ is of order ϵ^2.

To the next to leading order in ϵ the solutions of the equation are given under the convention that $\lambda_1 < \lambda_2 < \lambda_3$ by

$$
\begin{aligned}
\lambda_1 &= c_{12}^2 \delta_{21}, \\
\lambda_2 &= \delta_{31} - \frac{\delta_{31}}{1-\delta_{31}} \Big\{ s_{13}^2 + 2 c_{23} s_{13} \mathrm{Re}(\tilde{\varepsilon}_{e\tau} e^{i\delta}) \Big\} \\
\lambda_3 &= 1 + \frac{\delta_{31}}{1-\delta_{31}} \Big\{ s_{13}^2 + 2 c_{23} s_{13} \mathrm{Re}(\tilde{\varepsilon}_{e\tau} e^{i\delta}) \Big\} + s_{12}^2 \delta_{21}
\end{aligned}
\tag{A.24}
$$

In (A.24) we have ignored even smaller corrections to the lowest eigenvalue because it is of order ϵ^3.

We restrict ourselves to the leading order as was done by Cervera *et al.* [28] for the standard case without $\varepsilon_{\alpha\beta}$'s. To this order, we in fact do not need the order ϵ corrections in (A.24). By putting back the physical quantities replacing the scaled variables, the ν_μ

appearance probability can be expressed to order ϵ^2 as

$$
\begin{aligned}
P(\nu_e \to \nu_\mu; \varepsilon_{ee}, \varepsilon_{e\tau})|_{2nd} = {} & P(\nu_e \to \nu_\mu; \varepsilon = 0)|_{2nd} \\
& - \frac{4c_{23}s_{23}^2}{(\tilde{a} - \Delta m^2_{31})^2}\left[2\tilde{a}\Delta m^2_{31} s_{13}\mathrm{Re}(\varepsilon_{e\tau}e^{i\delta}) + c_{23}\tilde{a}^2|\varepsilon_{e\tau}|^2\right] \\
& \quad \times \cos\left(\frac{\tilde{a}L}{4E}\right)\sin\left(\frac{\Delta m^2_{31}L}{4E}\right)\sin\left(\frac{L}{4E}(\tilde{a} - \Delta m^2_{31})\right) \\
& + 4c_{23}s_{23}\left[\frac{(\Delta m^2_{31})^2}{(\tilde{a} - \Delta m^2_{31})^2}s_{23}\left(2s_{13}\mathrm{Re}(\varepsilon_{e\tau}e^{i\delta}) + c_{23}|\varepsilon_{e\tau}|^2\right)\right. \\
& \qquad \left. + \frac{2\Delta m^2_{31}\Delta m^2_{21}}{\tilde{a}(\tilde{a} - \Delta m^2_{31})}c_{12}s_{12}c_{23}\mathrm{Re}(\varepsilon_{e\tau})\right] \\
& \quad \times \cos\left(\frac{\Delta m^2_{31}L}{4E}\right)\sin\left(\frac{\tilde{a}L}{4E}\right)\sin\left(\frac{L}{4E}(\tilde{a} - \Delta m^2_{31})\right) \\
& + 4c_{23}s_{23}\left[c_{23}s_{23}|\varepsilon_{e\tau}|^2 - 2\frac{\Delta m^2_{21}}{\tilde{a}}c_{12}s_{12}c_{23}\mathrm{Re}(\varepsilon_{e\tau})\right] \\
& \quad \times \cos\left(\frac{L}{4E}(\tilde{a} - \Delta m^2_{31})\right)\sin\left(\frac{\tilde{a}L}{4E}\right)\sin\left(\frac{\Delta m^2_{31}L}{4E}\right) \\
& - \frac{8c_{23}s_{23}}{(\tilde{a} - \Delta m^2_{31})}\left[\Delta m^2_{31}s_{23}s_{13}\mathrm{Im}(\varepsilon_{e\tau}e^{i\delta}) + \Delta m^2_{21}c_{12}s_{12}c_{23}\mathrm{Im}(\varepsilon_{e\tau})\right] \\
& \quad \times \sin\left(\frac{\Delta m^2_{31}L}{4E}\right)\sin\left(\frac{\tilde{a}L}{4E}\right)\sin\left(\frac{L}{4E}(\tilde{a} - \Delta m^2_{31})\right), \qquad \text{(A.25)}
\end{aligned}
$$

where $P(\nu_e \to \nu_\mu; \varepsilon = 0)|_{2nd}$ is nothing but the Cervera *et al.* formula [28]

$$
\begin{aligned}
P(\nu_e \to \nu_\mu; \varepsilon = 0)|_{2nd} = {} & 4\frac{(\Delta m^2_{31})^2}{(\tilde{a} - \Delta m^2_{31})^2}s_{23}^2 s_{13}^2 \sin^2\left(\frac{L}{4E}(\tilde{a} - \Delta m^2_{31})\right) \\
& + 8J_r\frac{\Delta m^2_{31}\Delta m^2_{21}}{\tilde{a}(\tilde{a} - \Delta m^2_{31})}\sin\left(\frac{\tilde{a}L}{4E}\right)\sin\left(\frac{L}{4E}(\tilde{a} - \Delta m^2_{31})\right)\cos\left(\delta - \frac{\Delta m^2_{31}L}{4E}\right) \\
& + 4\left(\frac{\Delta m^2_{21}}{\tilde{a}}\right)^2 c_{12}^2 s_{12}^2 c_{23}^2 \sin^2\left(\frac{\tilde{a}L}{4E}\right). \qquad \text{(A.26)}
\end{aligned}
$$

It is notable that the NSI effects survive in the leading order, $\simeq \epsilon^2$. If one want to have explicit expression with $\varepsilon_{e\tau}$ and ε_{ee} one can just use the relations (A.5) in (A.25). The formula for $P(\nu_e \to \nu_\mu)$ is valid only for small $\varepsilon_{e\tau}$ but for any finite size ε_{ee}. The antineutrino probability can be obtained by the replacement $\delta \to -\delta$, $a \to -a$, and $\varepsilon_{\alpha\beta} \to \varepsilon^*_{\alpha\beta}$. We have checked that the same analytic formulas are obtained, when expressed in terms of observable physical quantities, even if we work in the intermediate energy region where $\lambda_2 > \lambda_3$.

Similarly, the formula of $P(\nu_e \to \nu_\mu)$ with $\tilde{\varepsilon}_{e\mu}$ can be computed to the leading order

as

$$
\begin{aligned}
P(\nu_e \to \nu_\mu;\varepsilon_{ee},\varepsilon_{e\mu})|_{2nd} = {} & P(\nu_e \to \nu_\mu;\varepsilon=0)|_{2nd} \\
& -\frac{4\tilde{a}s_{23}^3}{(\tilde{a}-\Delta m^2_{31})^2}\Big[2\Delta m^2_{31}s_{13}\mathrm{Re}(\varepsilon_{e\mu}e^{i\delta})+s_{23}\tilde{a}|\varepsilon_{e\mu}|^2\Big] \\
& \quad\times\cos\left(\frac{\tilde{a}L}{4E}\right)\sin\left(\frac{\Delta m^2_{31}L}{4E}\right)\sin\left(\frac{L}{4E}(\tilde{a}-\Delta m^2_{31})\right) \\
& +4\frac{(\tilde{a}-c_{23}^2\Delta m^2_{31})}{(\tilde{a}-\Delta m^2_{31})^2}\Big[2\Delta m^2_{31}s_{23}s_{13}\mathrm{Re}(\varepsilon_{e\mu}e^{i\delta})+(\tilde{a}-c_{23}^2\Delta m^2_{31})|\varepsilon_{e\mu}|^2 \\
& \qquad\qquad +2(\tilde{a}-\Delta m^2_{31})\left(\frac{\Delta m^2_{21}}{\tilde{a}}\right)c_{12}s_{12}c_{23}\mathrm{Re}(\varepsilon_{e\mu})\Big] \\
& \quad\times\cos\left(\frac{\Delta m^2_{31}L}{4E}\right)\sin\left(\frac{\tilde{a}L}{4E}\right)\sin\left(\frac{L}{4E}(\tilde{a}-\Delta m^2_{31})\right) \\
& +4c_{23}^3\left[c_{23}|\varepsilon_{e\mu}|^2+2\frac{\Delta m^2_{21}}{\tilde{a}}c_{12}s_{12}\mathrm{Re}(\varepsilon_{e\mu})\right] \\
& \quad\times\cos\left(\frac{L}{4E}(\tilde{a}-\Delta m^2_{31})\right)\sin\left(\frac{\tilde{a}L}{4E}\right)\sin\left(\frac{L}{4E}\Delta m^2_{31}\right) \\
& +\frac{8c_{23}s_{23}}{(\tilde{a}-\Delta m^2_{31})}\Big[\Delta m^2_{31}c_{23}s_{13}\mathrm{Im}(\varepsilon_{e\mu}e^{i\delta})-\Delta m^2_{21}c_{12}s_{12}s_{23}\mathrm{Im}(\varepsilon_{e\mu})\Big] \\
& \quad\times\sin\left(\frac{\Delta m^2_{31}L}{4E}\right)\sin\left(\frac{\tilde{a}L}{4E}\right)\sin\left(\frac{L}{4E}(\tilde{a}-\Delta m^2_{31})\right). \qquad \text{(A.27)}
\end{aligned}
$$

References

[1] Z. Maki, M. Nakagawa and S. Sakata,*Remarks on the unified model of elementary particles*, *Prog. Theor. Phys.* **28** (1962) 870;
B. Pontecorvo, *Neutrino experiments and the problem of conservation of leptonic charge*, *Zh. Eksp. Teor. Fiz.* **53** (1967) 1717 [*Sov. Phys. JETP* **26** (1968) 984].

[2] T. Kajita, *Atmospheric neutrinos*, *New J. Phys.* **6** (2004) 194;
A.B. McDonald, *Solar neutrino measurements*, *New J. Phys.* **6** (2004) 121 [astro-ph/0406253];
K. Inoue, *Reactor neutrino oscillation studies with KamLAND*, *New J. Phys.* **6** (2004) 147.

[3] L. Wolfenstein, *Neutrino oscillations in matter*, *Phys. Rev.* **D 17** (1978) 2369.

[4] J.W.F. Valle, *Resonant oscillations of massless neutrinos in matter*, *Phys. Lett.* **B 199** (1987) 432.

[5] M.M. Guzzo, A. Masiero and S.T. Petcov, *On the MSW effect with massless neutrinos and no mixing in the vacuum*, *Phys. Lett.* **B 260** (1991) 154.

[6] E. Roulet, *Mikheyev-Smirnov-Wolfenstein effect with flavor-changing neutrino interactions*, *Phys. Rev.* **D 44** (1991) 935.

[7] Y. Grossman, *Nonstandard neutrino interactions and neutrino oscillation experiments*, *Phys. Lett.* **B 359** (1995) 141 [hep-ph/9507344].

[8] Z. Berezhiani and A. Rossi, *Limits on the non-standard interactions of neutrinos from e^+e^- colliders*, *Phys. Lett.* **B 535** (2002) 207 [hep-ph/0111137].

[9] S. Davidson, C. Pena-Garay, N. Rius and A. Santamaria, *Present and future bounds on non-standard neutrino interactions*, *JHEP* **03** (2003) 011 [hep-ph/0302093].

[10] DELPHI collaboration, J. Abdallah et al., *Photon events with missing energy in e^+e^- collisions at $\sqrt{s} = 130\,GeV$ to $209\,GeV$*, *Eur. Phys. J.* **C 38** (2005) 395 [hep-ex/0406019].

[11] M.C. Gonzalez-Garcia, Y. Grossman, A. Gusso and Y. Nir, *New CP-violation in neutrino oscillations*, *Phys. Rev.* **D 64** (2001) 096006 [hep-ph/0105159].

[12] A.M. Gago, M.M. Guzzo, H. Nunokawa, W.J.C. Teves and R. Zukanovich Funchal, *Probing flavor changing neutrino interactions using neutrino beams from a muon storage ring*, *Phys. Rev.* **D 64** (2001) 073003 [hep-ph/0105196].

[13] P. Huber, T. Schwetz and J.W.F. Valle, *How sensitive is a neutrino factory to the angle θ_{13}?*, *Phys. Rev. Lett.* **88** (2002) 101804 [hep-ph/0111224].

[14] P. Huber, T. Schwetz and J.W.F. Valle, *Confusing non-standard neutrino interactions with oscillations at a neutrino factory*, *Phys. Rev.* **D 66** (2002) 013006 [hep-ph/0202048].

[15] T. Ota, J. Sato and N.-a. Yamashita, *Oscillation enhanced search for new interaction with neutrinos*, *Phys. Rev.* **D 65** (2002) 093015 [hep-ph/0112329].

[16] T. Ota and J. Sato, *Can ICARUS and OPERA give information on a new physics?*, *Phys. Lett.* **B 545** (2002) 367 [hep-ph/0202145].

[17] M.C. Gonzalez-Garcia et al., *Atmospheric neutrino observations and flavor changing interactions*, *Phys. Rev. Lett.* **82** (1999) 3202 [hep-ph/9809531];
M.C. Gonzalez-Garcia and M. Maltoni, *Atmospheric neutrino oscillations and new physics*, *Phys. Rev.* **D 70** (2004) 033010 [hep-ph/0404085].

[18] N. Fornengo, M. Maltoni, R.T. Bayo and J.W.F. Valle, *Probing neutrino non-standard interactions with atmospheric neutrino data*, *Phys. Rev.* **D 65** (2002) 013010 [hep-ph/0108043].

[19] A. Friedland, C. Lunardini and M. Maltoni, *Atmospheric neutrinos as probes of neutrino matter interactions*, *Phys. Rev.* **D 70** (2004) 111301 [hep-ph/0408264];
A. Friedland and C. Lunardini, *A test of tau neutrino interactions with atmospheric neutrinos and K2K*, *Phys. Rev.* **D 72** (2005) 053009 [hep-ph/0506143].

[20] S. Bergmann, M.M. Guzzo, P.C. de Holanda, P.I. Krastev and H. Nunokawa, *Status of the solution to the solar neutrino problem based on non-standard neutrino interactions*, *Phys. Rev.* **D 62** (2000) 073001 [hep-ph/0004049];
A. Friedland, C. Lunardini and C. Pena-Garay, *Solar neutrinos as probes of neutrino-matter interactions*, *Phys. Lett.* **B 594** (2004) 347 [hep-ph/0402266];
M.M. Guzzo, P.C. de Holanda and O.L.G. Peres, *Effects of non-standard neutrino interactions on MSW-LMA solution*, *Phys. Lett.* **B 591** (2004) 1 [hep-ph/0403134];
O.G. Miranda, M.A. Tortola and J.W.F. Valle, *Are solar neutrino oscillations robust?*, *JHEP* **10** (2006) 008 [hep-ph/0406280].

[21] H. Nunokawa, Y.Z. Qian, A. Rossi and J.W.F. Valle, *Resonant conversion of massless neutrinos in supernovae*, *Phys. Rev.* **D 54** (1996) 4356 [hep-ph/9605301];
H. Nunokawa, A. Rossi and J.W.F. Valle, *Supernova bounds on supersymmetric R-parity violating interactions*, *Nucl. Phys.* **B 482** (1996) 481 [hep-ph/9606445];
G.L. Fogli, E. Lisi, A. Mirizzi and D. Montanino, *Revisiting nonstandard interaction effects on supernova neutrino flavor oscillations*, *Phys. Rev.* **D 66** (2002) 013009 [hep-ph/0202269];

JHEP12(2007)002

A. Esteban-Pretel, R. Tomas and J.W.F. Valle, *Probing non-standard neutrino interactions with supernova neutrinos*, *Phys. Rev.* **D 76** (2007) 053001 [arXiv:0704.0032].

[22] N. Kitazawa, H. Sugiyama and O. Yasuda, *Will MINOS see new physics?*, hep-ph/0606013;
A. Friedland and C. Lunardini, *Two modes of searching for new neutrino interactions at MINOS*, *Phys. Rev.* **D 74** (2006) 033012 [hep-ph/0606101];
M. Blennow, T. Ohlsson and J. Skrotzki, *Effects of non-standard interactions in the MINOS experiment*, hep-ph/0702059.

[23] T. Hattori, T. Hasuike and S. Wakaizumi, *Flavor changing neutrino interactions and CP-violation in neutrino oscillations*, *Prog. Theor. Phys.* **114** (2005) 439 [hep-ph/0210138].

[24] M. Honda, N. Okamura and T. Takeuchi, *Matter effect on neutrino oscillations from the violation of universality in neutrino neutral current interactions*, hep-ph/0603268;
M. Honda, Y. Kao, N. Okamura, A. Pronin and T. Takeuchi, *Constraints on new physics from long baseline neutrino oscillation experiments*, arXiv:0707.4545.

[25] J. Kopp, M. Lindner and T. Ota, *Discovery reach for non-standard interactions in a neutrino factory*, *Phys. Rev.* **D 76** (2007) 013001 [hep-ph/0702269].

[26] J. Kopp, M. Lindner, T. Ota and J. Sato, *Non-standard neutrino interactions in reactor and superbeam experiments*, arXiv:0708.0152.

[27] S. Geer, *Neutrino beams from muon storage rings: characteristics and physics potential*, *Phys. Rev.* **D 57** (1998) 6989 [*Erratum ibid.* **D 59** (1999) 039903] [hep-ph/9712290];
A. De Rujula, M.B. Gavela and P. Hernandez, *Neutrino oscillation physics with a neutrino factory*, *Nucl. Phys.* **B 547** (1999) 21 [hep-ph/9811390].

[28] A. Cervera et al., *Golden measurements at a neutrino factory*, *Nucl. Phys.* **B 579** (2000) 17 [*Erratum ibid.* **B 593** (2001) 731] [hep-ph/0002108].

[29] Neutrino Factory/Muon Collider collaboration, C.H. Albright et al., *The neutrino factory and beta beam experiments and development*, physics/0411123.

[30] A. Blondel et al., *Future neutrino oscillation facilities*, *Acta Phys. Polon.* **B37** (2006) 2077 [hep-ph/0606111].

[31] J. Burguet-Castell, M.B. Gavela, J.J. Gomez-Cadenas, P. Hernandez and O. Mena, *On the measurement of leptonic CP-violation*, *Nucl. Phys.* **B 608** (2001) 301 [hep-ph/0103258].

[32] P. Huber and W. Winter, *Neutrino factories and the 'magic' baseline*, *Phys. Rev.* **D 68** (2003) 037301 [hep-ph/0301257].

[33] H. Minakata and H. Nunokawa, *Exploring neutrino mixing with low energy superbeams*, *JHEP* **10** (2001) 001 [hep-ph/0108085]; *CERN to Gran Sasso: an ideal distance for superbeam?*, *Nucl. Phys.* **110** *(Proc. Suppl.)* (2002) 404 [hep-ph/0111131].

[34] G.L. Fogli and E. Lisi, *Tests of three-flavor mixing in long-baseline neutrino oscillation experiments*, *Phys. Rev.* **D 54** (1996) 3667 [hep-ph/9604415].

[35] P. Huber, M. Lindner, M. Rolinec and W. Winter, *Optimization of a neutrino factory oscillation experiment*, *Phys. Rev.* **D 74** (2006) 073003 [hep-ph/0606119].

[36] Y. Kuno and Y. Okada, *Muon decay and physics beyond the standard model*, *Rev. Mod. Phys.* **73** (2001) 151 [hep-ph/9909265].

JHEP12(2007)002

[37] J. Barranco, O.G. Miranda and T.I. Rashba, *Probing new physics with coherent neutrino scattering off nuclei*, *JHEP* **12** (2005) 021 [hep-ph/0508299];
J. Barranco, O.G. Miranda, C.A. Moura and J.W.F. Valle, *Constraining non-standard interactions in $\nu_e e$ or $\bar{\nu}_e e$ scattering*, *Phys. Rev.* **D 73** (2006) 113001 [hep-ph/0512195];
J. Barranco, O.G. Miranda and T.I. Rashba, *Low energy neutrino experiments sensitivity to physics beyond the standard model*, *Phys. Rev.* **D 76** (2007) 073008 [hep-ph/0702175].

[38] K. Scholberg, *Prospects for measuring coherent neutrino nucleus elastic scattering at a stopped-pion neutrino source*, *Phys. Rev.* **D 73** (2006) 033005 [hep-ex/0511042].

[39] A. Bueno, M.C. Carmona, J. Lozano and S. Navas, *Observation of coherent neutrino-nucleus elastic scattering at a beta beam*, *Phys. Rev.* **D 74** (2006) 033010.

[40] O. Yasuda, *On the exact formula for neutrino oscillation probability by Kimura, Takamura and Yokomakura*, arXiv:0704.1531.

[41] H. Minakata and S. Uchinami, *On in situ determination of earth matter density in neutrino factory*, *Phys. Rev.* **D 75** (2007) 073013 [hep-ph/0612002].

[42] R. Gandhi and W. Winter, *Physics with a very long neutrino factory baseline*, *Phys. Rev.* **D 75** (2007) 053002 [hep-ph/0612158].

[43] V. Barger, D. Marfatia and K. Whisnant, *Breaking eight-fold degeneracies in neutrino CP-violation, mixing and mass hierarchy*, *Phys. Rev.* **D 65** (2002) 073023 [hep-ph/0112119].

[44] A. Cervera, *Physics potential of very long neutrino factory baselines*, talk given at *Eighth international workshop on the neutrino factories, superbeams, and beta beams*, University of California, Irvine U.S.A. (2006).

[45] H. Minakata and H. Nunokawa, *How to measure CP-violation in neutrino oscillation experiments?*, *Phys. Lett.* **B 413** (1997) 369 [hep-ph/9706281].

[46] M. Ishitsuka, T. Kajita, H. Minakata and H. Nunokawa, *Resolving neutrino mass hierarchy and CP degeneracy by two identical detectors with different baselines*, *Phys. Rev.* **D 72** (2005) 033003 [hep-ph/0504026];
T. Kajita, H. Minakata, S. Nakayama and H. Nunokawa, *Resolving eight-fold neutrino parameter degeneracy by two identical detectors with different baselines*, *Phys. Rev.* **D 75** (2007) 013006 [hep-ph/0609286].

[47] A. Cervera, F. Dydak and J. Gomez Cadenas, *A large magnetic detector for the neutrino factory*, *Nucl. Instrum. Meth.* **A451** (2000) 123.

[48] M. Campanelli and A. Romanino, *Effects of new physics in neutrino oscillations in matter*, *Phys. Rev.* **D 66** (2002) 113001 [hep-ph/0207350].

[49] K. Kimura, A. Takamura and H. Yokomakura, *Exact formula of probability and CP-violation for neutrino oscillations in matter*, *Phys. Lett.* **B 537** (2002) 86 [hep-ph/0203099]; *Exact formulas and simple CP dependence of neutrino oscillation probabilities in matter with constant density*, *Phys. Rev.* **D 66** (2002) 073005 [hep-ph/0205295].

[50] M. Blom and H. Minakata, *Unity of CP and T violation in neutrino oscillations*, *New J. Phys.* **6** (2004) 130 [hep-ph/0404142].

[51] Particle Data Group collaboration, W.M. Yao et al., *Review of particle physics*, *J. Phys.* **G 33** (2006) 1.

JHEP12(2007)002